A RAMAN SPECTROSCOPIC AND COMPUTATIONAL STUDY OF THE EFFECTS OF HALOGEN BONDING ON PYRIMIDINE CONTAINING SYSTEMS

By:
Peyton Lindsey Reves

A thesis submitted to the faculty of The University of Mississippi in partial fulfillment of the requirements of the Sally McDonnell Barksdale Honors College.

Oxford
May 2015

Approved by

_____
Advisor: Professor Nathan Hammer

_____
Reader: Professor Gregory Tschumper

_____
Reader: Professor Davita Watkins

ACKNOWLEDGEMENTS

First, I would like to thank my parents, Dennis and Sandra Reves, and my brother, Cooper Reves, for supporting me throughout my academic career. Many people, both students and professors, have shown me tremendous support during the time I worked on the research presented here. I would like to thank these people for challenging me during my undergraduate curriculum and motivating me to become a better student and chemist. I would also like to thank the other members of my research group, specifically John Kelly, Louis McNamara, and Katelyn Allen, for their endless help and support during the course of this research. Additionally, I would like to thank Dr. Davita Watkins who provided my inspiration for the concept this research is focused on. I would also like to thank Dr. Gregory Tshumper for his assistance with the computational portion of this research. I would like to thank the Sally McDonnell-Barksdale Honors College for providing me with countless opportunities here at the University of Mississippi. Lastly, I would like to thank my advisor, Dr. Nathan Hammer, for aiding me in my research every step of the way and allowing me to work in his research lab.

ABSTRACT

PEYTON LINDSEY REVES: A Raman Spectroscopic and Computational Study of the Effects of Halogen Bonding on Pyrimidine Containing Systems
(Under the direction of Dr. Nathan Hammer)

This thesis involves the study of the effects of halogen bonding on pyrimidine containing systems. Halogen bonding is a type of non-covalent interaction that can occur when a Lewis base interacts with an iodine, bromine, or chlorine atom in a second molecule. The phenomenon of halogen bonding is explained by the presence of a localized region of positive electrostatic potential that exists on the halogen. This positive region is referred to as the σ-hole, and gives halogen bonding its other common name, σ-hole bonding. The magnitude of the positive σ-hole depends on both the type of halogen molecule involved in the interaction as well as the characteristics of the molecule to which the halogen is bonded. The strength of the halogen bond tends to increase from chlorine < bromine < iodine. The careful and directed use of this intermolecular interaction has been suggested for use in several areas of supramolecular chemistry. For example, halogen bonding has been employed in crystal engineering as a means of forming new types of crystals. In this work, halogen bonding interactions between a nitrogen-containing heterocyclic biological building block (pyrimidine) and aryl halides are studied both experimentally and theoretically. Experimental Raman spectra of liquid mixtures are compared to the results of electronic structure calculations on halogen bond containing molecular clusters. Mixtures pyrimidine with bromobenzene, iodobenzene, bromopentafluorobenzene, and iodopentafluorobenzene were examined both experimentally and theoretically. Results indicate that the addition of electron withdrawing fluorine atoms strengthen the halogen bond interaction, leading to significant blue shifts in a number of pyrimidine's normal modes in mixtures of iodopentafluorobenzene and pyrimidine, similar to the shifts induced by hydrogen bonding between pyrimidine and water. Additionally, a co-crystal containing halogen bonds is characterized using micro-Raman spectroscopy and compared to theoretical calculations of the co-crystal complex. Though only small shifts in vibrational modes were observed in the co-crystal, theory and experiment proved to agree very well. An X-Ray crystal structure of the co-crystal, however, confirmed the presence of halogen bonds in the crystal.

Table of Contents

LIST OF FIGURES AND TABLES

LIST OF ABBREVIATIONS

Py-Pyrimidine

C_6H_5Br-Bromobenzene

C_6H_5I-Iodobenzene

C_6F_5Cl-Chloropentafluorobenzene

C_6F_5Br-Bromopentafluorobenzene

C_6F_5I-Iodobenzene

Chapter 1: Noncovalent Interactions and Halogen Bonding

1.1 Noncovalent Interactions

Noncovalent interactions serve a vital role in all areas of chemistry. Before discussing non-covalent interactions, the definition of a covalent bond must be established. A covalent bond is formed when two systems with unfilled electronic shells overlap; when this occurs, the electron density between the two systems increases which forms a bond. When electron density increases in this region the bond strength increases. Non-covalent interactions arise from other properties of a system, which can include induced, permanent, and instantaneous multipoles that can exist in a system which result in attraction or repulsion between systems. Electrostatic interactions arise in systems that contain permanent multipoles; these multipoles (monopoles, dipoles, quadrapoles, etc.) interact with each other, with the energy contribution usually dominating over other types of non-covalent interactions. Induction, or polarization, interactions occur when permanent and induced multipoles interact with each other. The permanent multipole of one system induces a multipole on another, allowing an interaction to occur. Dispersion interactions take into account the existence of instantaneous multipoles that can exist in a system due to the oscillations of nuclei and electron clouds. Specifically, instantaneous

multipoles can induce a multipole in another system, allowing an interaction to occur. Another name for dispersion interactions are van der Waals interactions, which occur due to these instantaneous multipoles that can exists in a system. Van der Waals are weak interactions found in all molecules that involve the electrons surrounding the molecule. Though initially believed to have a small energy contribution and therefore a small part in stabilization of systems, it has now been shown that dispersion forces play a substantial roll in stabilization.

The three energy contributions mentioned above, induction, electrostatic, and dispersion, all can be attractive in nature and must be balanced by a corresponding repulsive force. This repulsive force is quantum mechanical in nature and is referred to as exchange-repulsion energy. This energy is also called Pauli repulsion, and is related to the Pauli exclusion principle. Electron density increases in antibonding orbitals, which results in a repulsion between the two systems. Charge transfer can also occur between two systems due to nonzero overlap of electron clouds, from the electron donor to the electron acceptor. In the specific case of the non-covalent interaction hydrogen bonding, this transfer occurs between the proton donor and the proton acceptor. The overall effect of these non-covalent interactions is the stabilization of the interacting systems. The energy of the total system is lower than the sum of the individual systems.

Hydrogen bonding is commonly thought of as a special type of non-covalent interaction, however, this is not the case. The interactions and charge transfer observed in hydrogen bonded complexes can also be observed in other systems that are stabilized by the exact same non covalent interactions. The most important energy contribution is electrostatic which is also accompanied by induction and dispersion contributions. All of

these contributions are balanced by exchange repulsions; this same energy breakdown can be observed in other non-covalent systems. The unique characteristic of hydrogen bonding comes from the sharing of the hydrogen atom between two highly electronegative atoms. The hydrogen atom is attached to an electronegative atom which draws electron density away from the hydrogen, leaving the hydrogen with a slightly positive charge. Interacting atoms are usually highly electronegative with the ability to donate electron density to the partially positive hydrogen atom. This sharing weakens the bond between the hydrogen atom and the electronegative atom it is covalently bound too, leading to interesting results.[1] Figure 1.1.1 below shows an example of a hydrogen bond involving nitrogen, with the yellow dotted line representing the hydrogen bond.

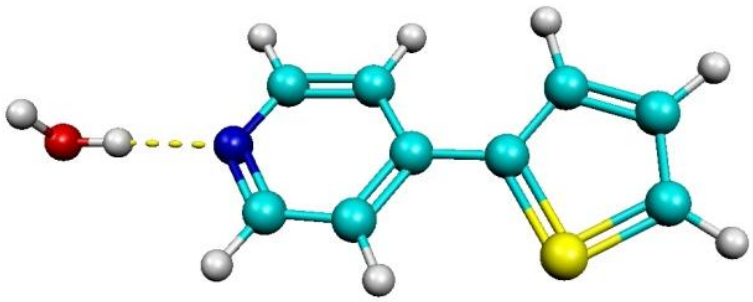

Figure 1.1.1: Example of a hydrogen bonded complex involving water and Pyridyl-Thiophene

The strength of non-covalent interactions is commonly referred to by its binding energy. This energy refers to the total energy due to the non-covalent interaction that is occurring. Hydrogen bonds usually have binding energies ranging from -4 to -10 kilocalories per mole, with multiple hydrogen bonds in one system contributing more energy.[2] Examining this binding energy can give information about the strength of the non-covalent interaction that is occurring.

As discussed, hydrogen bonding is not a special case of a non-covalent interaction, but rather is a combination of the nearly limitless types of non-covalent interactions that may occur in a system due to dispersion, induction, and electrostatic interactions. A non-covalent interaction that is similar in formation to hydrogen bonding is known as halogen bonding, and will be discussed in the next section of this thesis.

1.2 Halogen Bonding

Halogen bonding is a unique and relatively newly focused on type of noncovalent interaction that has garnered considerable interest in recent years due to its potential applications. Halogen bonding is referred to as the noncovalent interaction that can occur between halogen atoms, X, on a molecule with a region of electron density on another molecule.[3] The halogen usually acts as a Lewis acid, accepting electron density from the Lewis base that it interacts with.[4] The strength of the interaction increases from fluorine, to chlorine, to bromine, to iodine, with iodine halogen bonding interactions being the strongest in nature.[3] This interaction increases in this manner because the relative polarizability of the atom increases from chlorine, to bromine, to iodine. This increased polarizability means that outer electrons can move more freely, thus allowing for a larger positive region to be formed in iodine containing complexes.This interaction can occur due to a region of positive electrostatic potential that is present on the halogen atom. Shown below in Figure 1.2.1 are electrostatic potential maps of C_6F_5Cl, C_6F_5Br, and C_6F_5I.

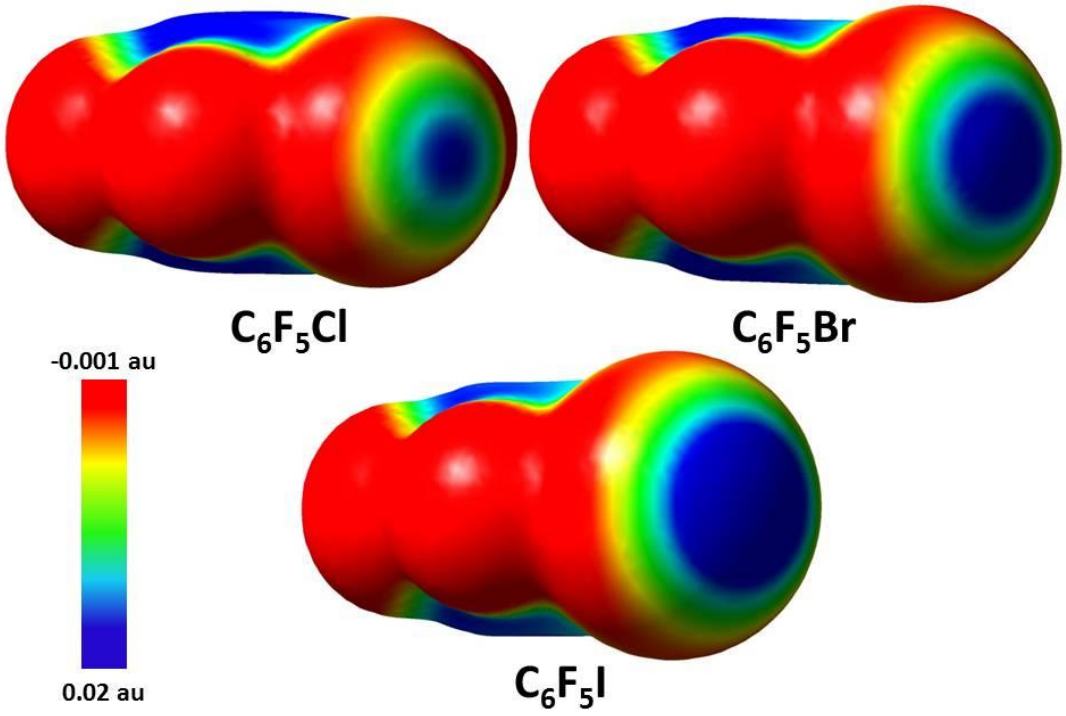

Figure 1.2.1: Electrostatic Potential Maps of C_6F_5Cl, C_6F_5Br, and C_6F_5I[1]

As can be seen in Figure 1.2.1 above, a ring of negative charge, shown in red, surrounds the halogen atom. A region of electropositive charge is oriented on the axis of the covalent bond linking the halogen to the rest of the molecule on the outer portion of the halogen atom; this positive region is shown in Figure 1.2.1 as the blue region. The presence of this positive region is due to this uneven distribution of electron density. This region of positive charge is called a sigma hole, which gives halogen bonding its other name, sigma-hole bonding.[1] As can be seen in Figure 1.2.1, the size of this positive region increases from chlorine, to bromine, to iodine, as predicted by halogen bonding theory. In the earliest studies of halogen bonding, it was thought that fluorine would not form a sigma hole due its lack of polarizability and its high electronegativity. However,

[1] B3LYP/def2-TZVPD

recent studies have shown that fluorine can in fact form a positive sigma hole if bonded to groups that are highly electron withdrawing. Though the magnitude of the sigma hole on fluorine in these types of compounds is considerably smaller than seen in other halogens, it has been shown to form halogen bond containing complexes.[5] Shown below in Figure 1.2.2 is a complex containing a halogen bond, with the yellow dotted lines representing the halogen bond.

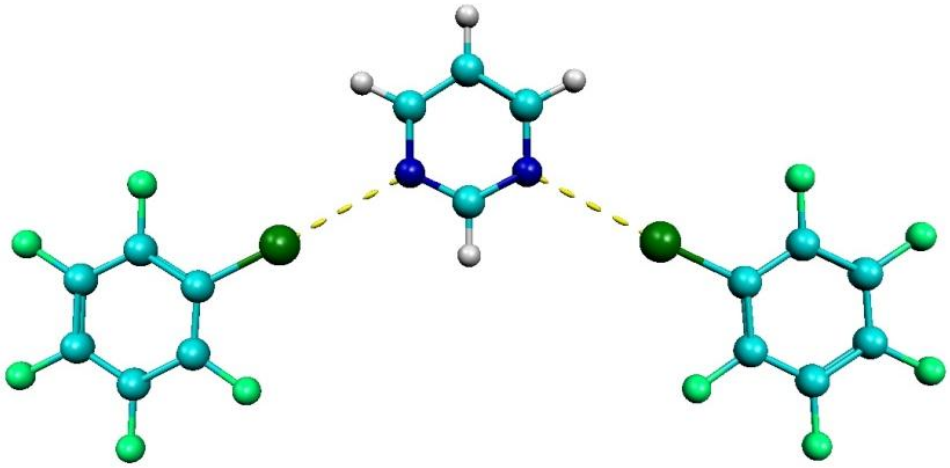

Figure 1.2.2: Halogen bonded complex between Pyrimidine and C_6F_5Br

The tunability of halogen bond interactions is another reason it has been of recent focus, due to potential application of complexes containing halogen bonds. The magnitude of the sigma hole on a halogen atom can be increased by electron withdrawing groups bonded to the remainder of the molecule, leading to stronger halogen bond interactions.[6] In particular, molecules containing the highly electronegative and electron withdrawing atom fluorine have been shown to be of particular use in halogen bond studies. The substitution of hydrogen with fluorine in chlorine ,bromine, or iodine containing molecules has been shown to produce halogen bond interactions that are up to 100% stronger due to the larger magnitude of the sigma hole on the halogen.[7] The

binding energies of fluorinated chlorine, bromine, and iodine complexes with NH_3 have been studied theoretically, with values ranging up to -5.8 kilocalories per mole. [8] The atoms that serve as the site of interaction for halogen bonding are usually nitrogen, oxygen, or sulfur, with nitrogen usually resulting in stronger halogen bond interactions. Nitrogen results in a stronger interaction because it more easily donates electron density in these types of interactions. Halogen bonds have also been of interest in biochemical and biophysical studies involving using halogen bonding as a means of directing confirmation of biological molecules. In a recent study, a halogen bond was engineered to direct the confirmation of a biological molecule, in this case a portion of DNA. This study showed that halogen bonding interactions dominated hydrogen bonding interactions with an energy 2-5 kilocalories per mole stronger than the hydrogen bond energy. This study and similar studies shed light on how halogen bonding can be utilized in the design and construction of a variety of molecular complexes.[9] In a study concerning halogen bonding in biological molecules, Auffinger found that the majority of halogen bonding interactions in biological environments occurred with carbonyl oxygen and not with nitrogen.[10] Another focus of studies concerning halogen bonding has been to examine the similarities between hydrogen bonding and halogen bonding. It has been found that "practically all the energetic and geometric features know for hydrogen bond complexes are encountered in halogen bond complexes as well." [11] A main difference between the two types of interactions, however, is due to the size of halogens, steric hindrance is a bigger issue than in hydrogen bonding.[11] Information regarding the directionality of halogen bonding complexes obviously became a focus as more was learned about the interaction itself. Valuable information about the interaction can be

found using X-Ray structural analysis. The angle between the halogen bond axis and the acceptor atom has been found to usually be around 180° which was found by analyzing X-Ray crystal structures of halogen bond containing complexes.[12] Halogen bond containing co-crystals have also shed more light onto the similarities between hydrogen bonding and halogen bonding. In one study, the same Lewis base was used to grow a co-crystal containing halogen bonds and a co-crystal containing hydrogen bonds. When melting points of the crystals were taken, the crystals containing halogen bonds had a considerably higher melting point than their hydrogen bonded counterpart. Though this difference could also be from different structural packing effects in the crystals, this suggests that halogen bond containing crystals are much more stable than those containing hydrogen bonds.[13]

The first study that showed the ability of halogens to interact with electron donating groups was published in 1863 by Guthrie. This paper described interactions he observed between ammonia and iodine complexes, complexes he refers to as iodide of iodammonium. These complexes first caught Guthrie's attention after previous studies with ammonia and iodine had produced different compounds based on the reaction conditions of the ammonia and iodine. He concluded that the conditions the products were prepared in had a large influence on the properties and composition of the compound that resulted. He found, using his own method, that the previous studies had actually incorrectly identified the resulting compound, which he described and called iodide of iodammonium. Guthrie inferred that this complex contained an interaction between iodine and the nitrogen on ammonia, which later scientists analyzed and found to be the first indisputable case of the interaction of a halogen with an electron donor. [14]

The next mention of this type of interaction came in 1896, when Remsen and Norris published a study concerning interactions between halogens and methylamines, which included dimethylamine and trimethylamine. Initially, Remsen and Norris were attempting to create a selenium salt containing bromine, but instead obtained a precipitate they were not expecting. After analyzing this precipitate and finding that it did not contain selenium but did contain bromine, they decided to further investigate the interaction they believed to be occurring. Their experiments included studying how chlorine, bromine, and iodine interacted with both diethyl and triethyl amine.[15] These two studies were the earliest mentions of halogen interactions with electron donating groups on other molecules, which would eventually lead to further interest in halogen interactions and eventually, the creation of the term halogen bond.

Chapter 2: Spectroscopy

2.1 Definition of Spectroscopy

Spectroscopy is defined at the interactions between light and matter. Light can have different effects on the matter it interacts with based on its inherent properties. Spectroscopy can be used to determine fundamental physical and chemical properties of a substance based on interaction with light.[16]

2.2 Electromagnetic Radiation

Light is also known as electromagnetic radiation, and exhibits characteristics of both a particle and a wave; this is known as the wave-particle duality of light. Light can be represented as a series of oscillating perpendicular magnetic and electric fields. Initially, light was only known by its wave nature, however, later studies revealed that light also had qualities of a particle. Particles of light are referred to as photons, and are characterized by their energy. Equation 2.2.1, below, illustrates how the energy of a photon, a particle, is defined by wavelength and frequency, showing that a particle can act as a wave.

$$E = h\nu = \frac{hc}{\lambda} \qquad (2.2.1)$$

In equation 1.1, h is defined as Planck's constant with a value of 6.626 x 10^{-34} J s, ν is frequency, c is the speed of light 3.00 x 10^{8} m/s, and λ defined as the wavelength of the light. As shown in this equation, the energy of a photon is directly proportional to the frequency of the light and inversely proportional to the wavelength of the light. The formulation of this equation demonstrated the wave-particle duality of light, and how the energy of a photon is related to its wave characteristics. Electromagnetic radiation can range from high energy, short wavelength and high frequency, to low energy, long wavelength and low frequency.[16] The range of electromagnetic radiation is known as the electromagnetic spectrum, shown below in Figure 2.2.1.

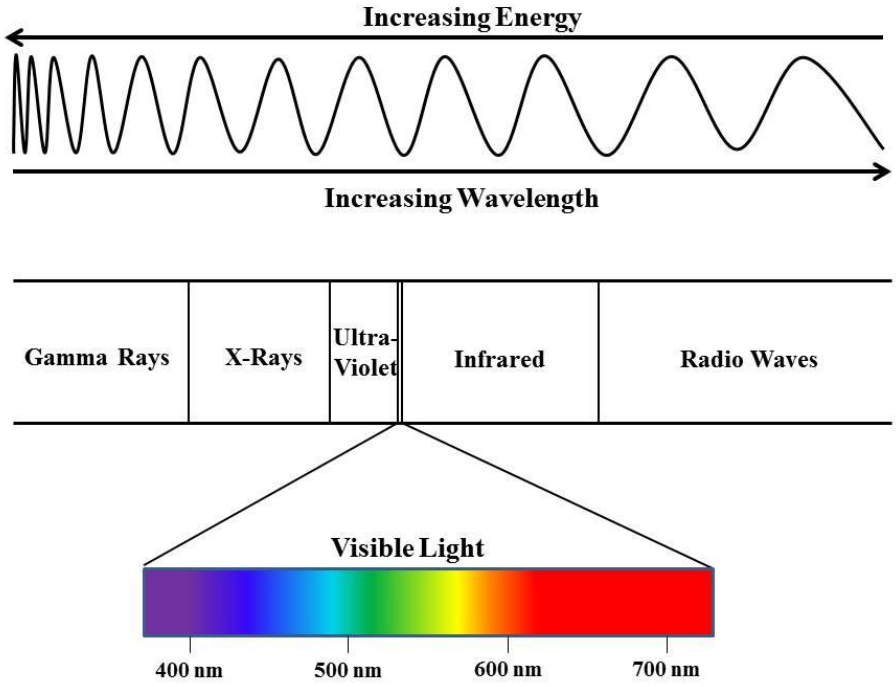

Figure 2.2.1: The Electromagnetic Spectrum

As shown in Figure 3, the actual range of light that can be seen by the human eye is a very small portion of the electromagnetic spectrum. However, many other portions of the electromagnetic spectrum do prove to be useful to chemists in spectroscopic analysis.[16]

Understanding the basics of electromagnetic radiation is crucial when understanding how incident light interacts with matter. When incident light hits matter, transitions between energy levels occur. There are three processes by which these transitions can occur: absorption, stimulated emission, and spontaneous emission. Absorption occurs when an incident photon prompts a transition to a higher energy level, while emission occurs when a photon is emitted due to the molecule relaxing to a lower energy level. Specifically, spontaneous emission is the result of a system in an excited state spontaneously transitioning to a ground state, while stimulated emission occurs when an incident photon causes a system to transition from an excited state to the ground state. Figure 2.2.2, below, shows an illustration of this process. The upward pointing red lines correspond to an incident photon, while the downward pointing red lines correspond to an emitted photon.

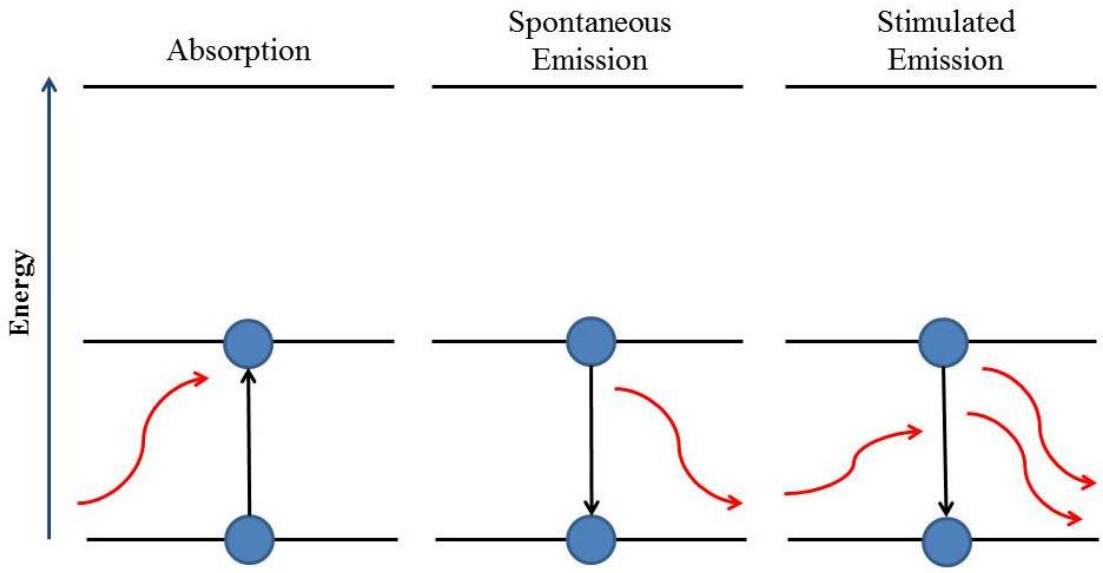

Figure 2.2.2: Illustration of Absorption, Spontaneous Emission, and Stimulated Emission

These three processes are described by the Einstein Coefficients, B_{12} (absorption), B_{21} (stimulated emission), and A_{21} (spontaneous emission). These coefficients correspond to the rate at which these processes occur. Absorption and stimulated emission are proportional to $\rho(\nu)$, which is the spectral density as a function of frequency, due to fact that they both occur due to incident photons. Spontaneous emission, however, is independent of the spectral density; it is dependent on the lifetime of the excited state in a molecule. The rate of these three processes is also directly proportional to the number of molecules in the state in which the transition originated. These three processes and their relative rates are illustrated below in Figure 2.2.3.

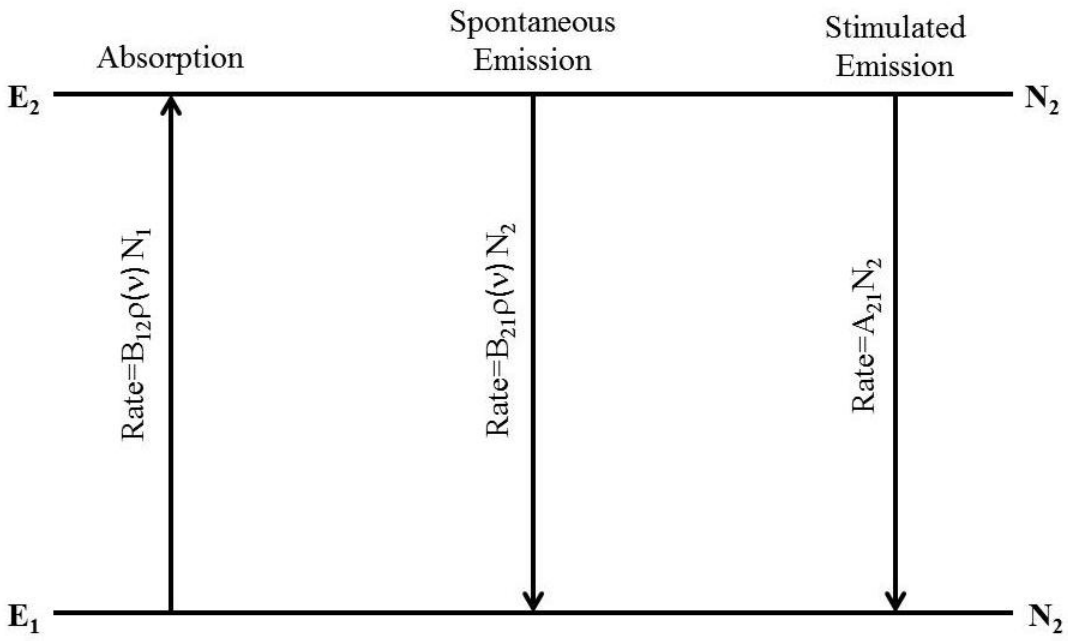

Figure 2.2.3: Illustration showing the rates of Absorption, Spontaneous Emission, and Stimulated Emission

At equilibrium, the rate of transition from 1 to 2 must be equal to the rate of transition from 2 to 1. Therefore, the sum of both spontaneous and stimulated emission must be equal to absorption. Following this logic, Einstein concluded that the ratio of spontaneous emission to stimulated emission is directly proportional to the frequency cubed, which is shown below in Equation 2.2.2.

$$\frac{A_{21}}{B_{21}} = \frac{16\pi^2 h\upsilon^3}{c^3} \tag{2.2.2}$$

It can be gathered from this equation that as frequency increases the rate of spontaneous emission increases, competing with the amount of stimulated emission. This fact becomes very important when designing light sources used in spectroscopy. Light

emitted via spontaneous emission is incoherent, that is, their phases are in random. Light emitted via stimulated emission is coherent with all photons in phase. A laser is a coherent light source, and so the relationship illustrated in Equation 1.3.1 is very important when designing a laser to be used as a light source. As the light source used in this experiment is a laser, this concept is very important to fully understand.[17]

As previously mentioned, the populations of the lower and upper state also affect the rate of these three processes. The relative populations, N_1 and N_2, are related to each other by the Boltzmann distribution, shown below in Equation 2.2.3.

$$\frac{N_2}{N_1} = e^{-(E_2-E_1)/kT} \tag{2.2.3}$$

E_1 and E_2 refer to the relative energies of the levels, which are equal to hν, or Planck's constant multiplied by frequency. T refers to temperature in Kelvin, while k refers to the Boltzmann constant which is equal to 1.381 x 10^{-23} J/K. The result of this calculation is the ratio of molecules in the excited state to molecules in the ground state.[18]

2.3 Vibrational Spectroscopy

Vibrational spectroscopy analyzes the vibrational motions of molecule, with information regarding the vibrational modes of a molecule giving insight into molecular structure and interactions with other molecules. Quantum mechanics describes vibrational motions using the harmonic oscillator model and uses the time-independent Schrödinger equation as a means of determining vibrational energy levels of a molecule. Generally, the only observable transition in vibrational spectroscopy is from the ground state to the first excited states. However, there are many different transitions that may occur but may not

be observed. Selections rules exist for every type of spectroscopy and determine transitions that can occur between states in a molecule. The selection rules for vibrational spectroscopy are derived based on the quantum mechanical harmonic oscillator, and are given as the transition dipole integral. The transition dipole integral is show below in Equation 2.3.1.

$$\mu_x^{mn} = \int \psi_m^*(x)\mu_x(x_e + x)\,\psi_n(x)dx \neq 0 \qquad (2.3.1)$$

An approximation of energy levels and transitions can be made using the potential energy diagrams; this is shown below in Figure 2.3.1.[18]

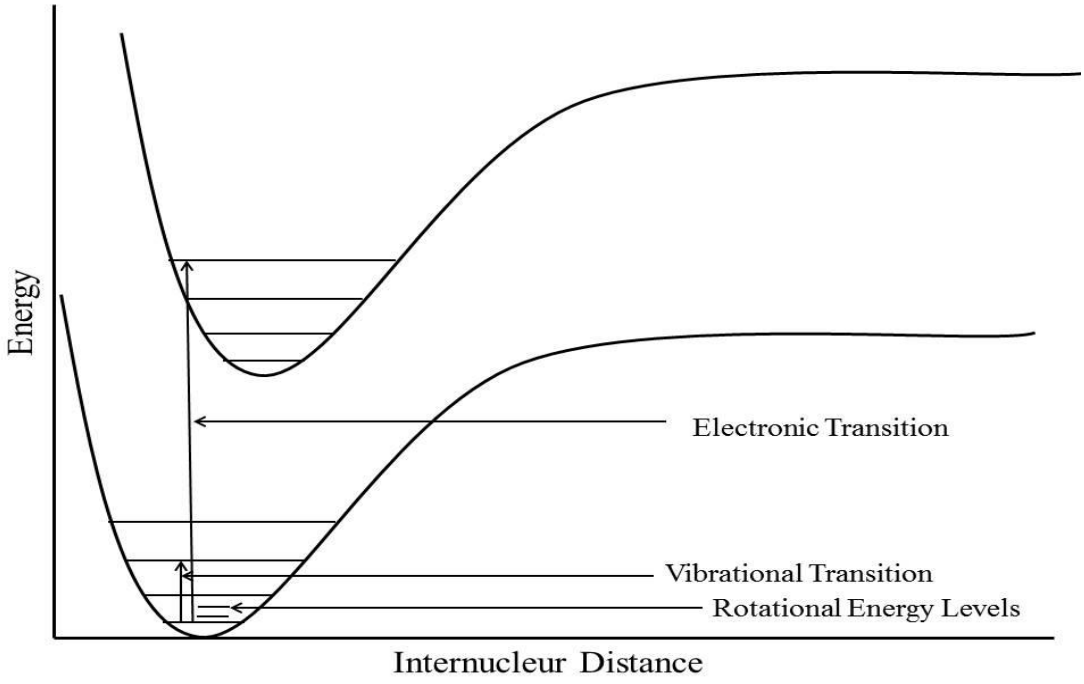

Figure 2.3.1: Potential energy diagram showing energy levels and transitions

There are two types of molecular vibrations: bending and stretching. Stretching motions can be symmetrical or asymmetrical, while bending motions may be scissoring, rocking, wagging, or twisting. An illustration of these motions is shown below in Figure 2.3.2.

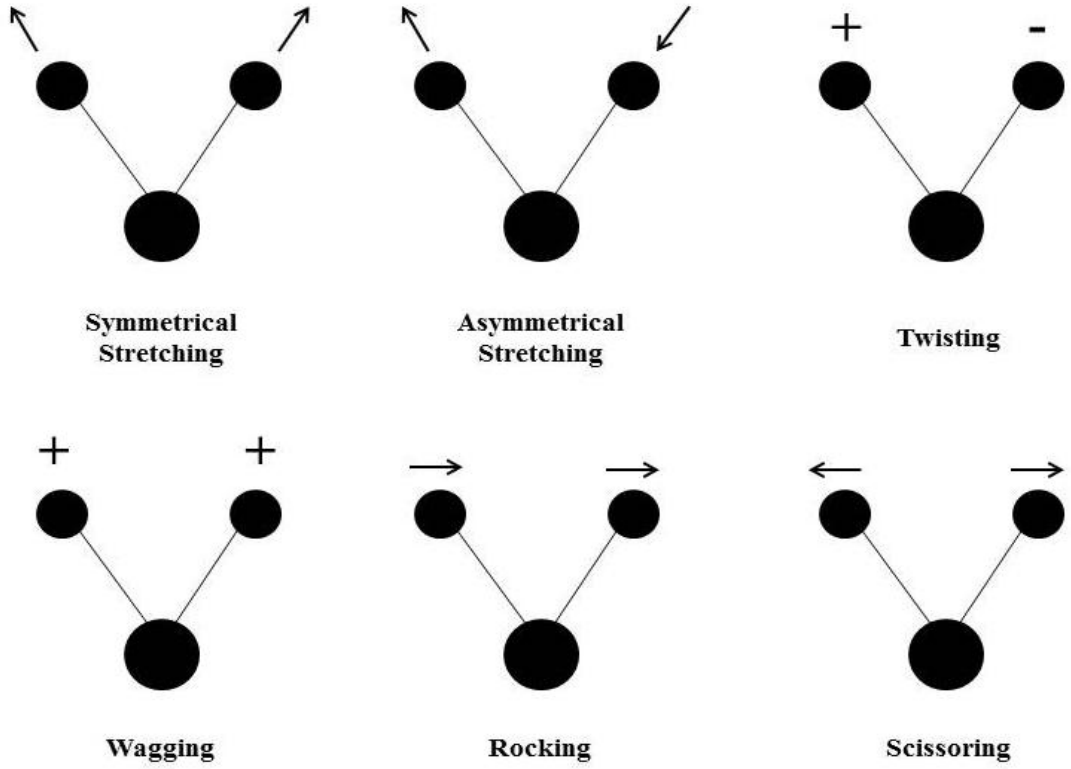

Figure 2.3.2: Example Vibrational Motions

Molecules have a different number of vibrational modes based on if the molecule is linear or non-linear. Linear molecules have a total of 3N-5 vibrational modes, while non-linear molecules have a total of 3N-6 vibrational modes, with N equal to the number of atoms in the molecule. Each vibrational mode in a molecule has an associated energy that is seen as a peak on a spectrum, giving information about the inherent characteristics of the molecule.[16]

2.4 Computational Methods

Computational methods used in this study to obtain theoretical results of the complexes studied experimentally are based in quantum mechanical theory. Mathematically, the interactions between matter and electromagnetic radiation can be determined using the time independent Schrödinger equation. The general form of this equation is shown below in Equation 2.4.1.

$$\hat{H}\psi_n = E\psi_n \qquad (2.4.1)$$

$\hat{H}$ is the Hamiltonian, or the total energy operator of the system of interest. ψ is the wavefunction of the system, which describes the state of a particle in three dimensions. E represents the energy of the state being analyzed, while n represents the quantum number.[18] The computational program used in this study, Gaussian 09, approximates solutions to the time independent Schrödinger for multiple electron systems being analyzed by the program.[19] The Schrödinger equation cannot be completely solved for systems containing more than one electron.

These calculations more specifically search the potential energy surface (a plot of energy calculated for various values of bond length) for a stationary point in the energy value. This stationary point corresponds to the lowest energy geometrical configuration of the molecule or molecular complex. This occurs during the optimization step of the calculation. Further evaluation of the complex by calculating vibrational frequencies gives more information about the specific geometrical configuration at that specific stationary point in the potential energy surface. A minimum is a stationary point with 3N-6 vibrational frequencies. A transition state is a minimum with one imaginary frequency.

A minimum with no imaginary frequencies suggest that the geometrical configuration present there is the lowest energy geometrical configuration of that molecule or molecular complex.

As part of these computational studies a method and basis set must be defined before the calculation can be carried out. The basis sets are a group of mathematical functions that define the orbitals of the molecule. One basic function resembles an atomic orbital. A linear combination of atomic orbitals is one method used to form molecular orbitals, and so a combination of these basis functions forms the molecular orbital used in the calculation. Larger basis sets have more basis functions in them, allowing for a more accurate representation of molecular orbitals and therefore a more accurate final result. Different types of basis functions are also needed in order to obtain more accurate results from calculations. Polarization functions and diffuse functions are additional types of functions that can provide more accurate results based on the type of molecule or molecular complex being analyzed.

Density functional theory forms the theoretical background of the theory used in these calculations Density functional theory is based on the fact that energy is a functional of the electron density. The specific method used in this theoretical analysis is the B3LYP method. The B refers to the Becke correction, which incorporates the fact that density can vary greatly in a molecule. The L, Y, and P refer to Lee, Yang, and Parr who later suggested a "gradient corrected correlation functional". The BLYP method came before B3LYP, and refers to the joint use of the Becke correction and the LYP correction. The 3 refers to another layer of theory added in which forms a hybrid functional.[20-22]

Vibrational frequencies are calculated by Gaussian 09 by determining force constants, then using those force constants to calculate the vibrational frequencies. The keyword "freq" is used to indicate to the program that this analysis should be carried out. This keyword, however, only calculated the frequencies and the infrared intensities of those frequencies. The infrared intensities are determined by the dipole derivatives. The keyword "freq=raman" however, is used to determine the Raman intensities of the vibrational frequencies. This keyword was used in these calculations as the experimental data was Raman spectra. The Raman intensities are determined by differentiating the dipole derivatives with respect to an electric field, which results in polarizability derivatives. These polarizability derivatives are then used to determine the Raman intensities of the vibrational frequencies.[23]

Chapter 3: Raman Spectroscopy Principles and Instrumentation

3.1 Principles of Raman Spectroscopy

Raman spectroscopy is a technique used to study molecular vibrations via light scattering. In order for a vibrational mode to be Raman active, it must have a net change in polarizability during the vibration. Raman spectroscopy is often thought of as a complement to Infrared spectroscopy, which also studies vibrational modes of molecules. In order for a vibrational mode to be active in Infrared spectroscopy, the molecule must have a net change in dipole moment. Therefore, some vibrational modes, such as a symmetric stretching mode, will not have a change in dipole moment and will therefore not be IR active. This mode does, however, have a net change in polarizability and is therefore Raman active. Typically, symmetric modes have a high intensity in Raman spectroscopy while asymmetric modes are weak in intensity if they are observed at all.

In Raman spectroscopy, a monochromatic light source, usually a laser, excites the molecule of interest to a virtual energy level. When the molecule relaxes from this virtual energy level, the light is scattered in one of three ways. The first, Rayleigh scattering, occurs when incident light and molecules interact elastically with no energy

lost during the collision. The scattered light is of the same wavelength and energy as the incident light. Rayleigh scattering accounts for the overwhelming majority of scattered light, however, one in every million photons interacts inelastically with molecules of interest. Stokes scattering occurs when the molecule is excited to a higher vibrational state by the incident light, with the scattered light being of longer wavelength and lower energy than the incident light. Stokes scattering is the scattered light most commonly detected in Raman spectroscopy. Anti-Stokes scattering occurs when incident light causes the molecule to relax to a lower vibrational state, with the scattered light being of shorter wavelength and higher energy than the incident light.[16] A diagram of this phenomenon is shown below in Figure 3.1.1.

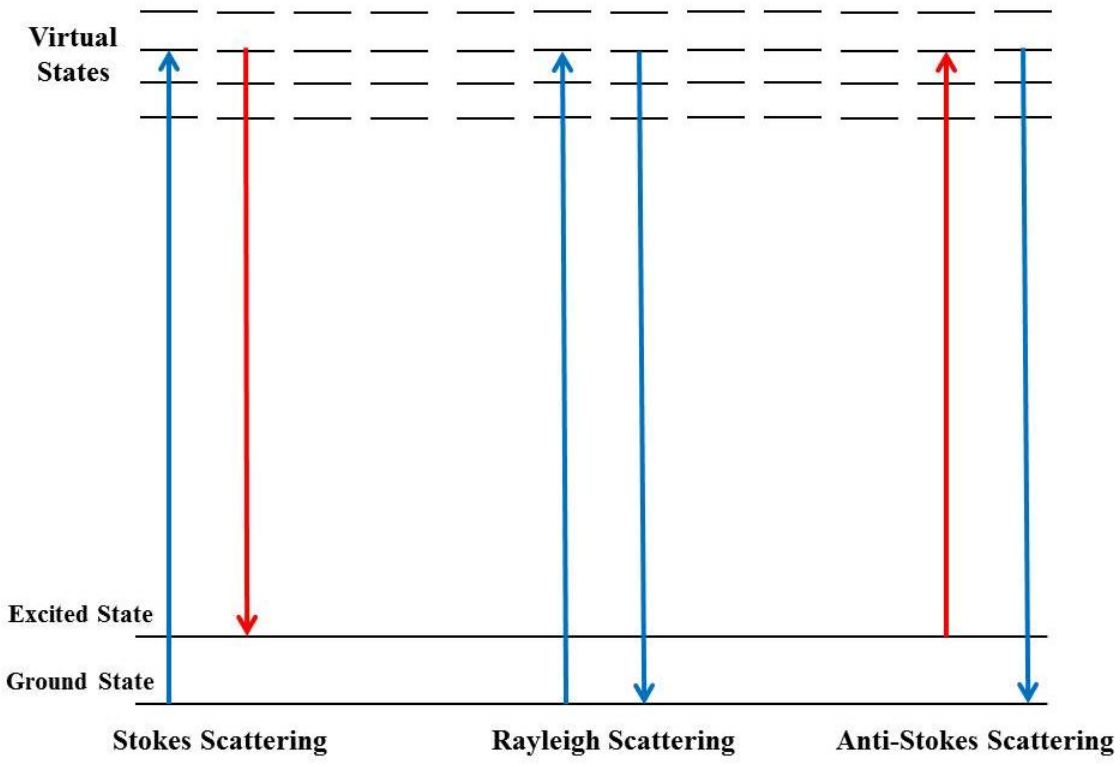

Figure 3.1.1: Schematic of Rayleigh, Stokes, and Anti-Stokes Scattering

Shifts in vibrational modes that are observed in Raman spectroscopy are commonly referred to as red and blue shifts. Though these terms are not technically accurate and are a product of history, they are still used today as a means of describing observed spectral changes. A red shift corresponds to a shift to lower energy, while a blue shift corresponds to a shift to higher energy.[24]

3.2 Raman Spectroscopy Instrumentation

A traditional Raman spectrometer requires a light source, a sample holder, a monochromator, and a detector. A simple box diagram of a Raman spectrometer is shown below in Figure 3.2.1.

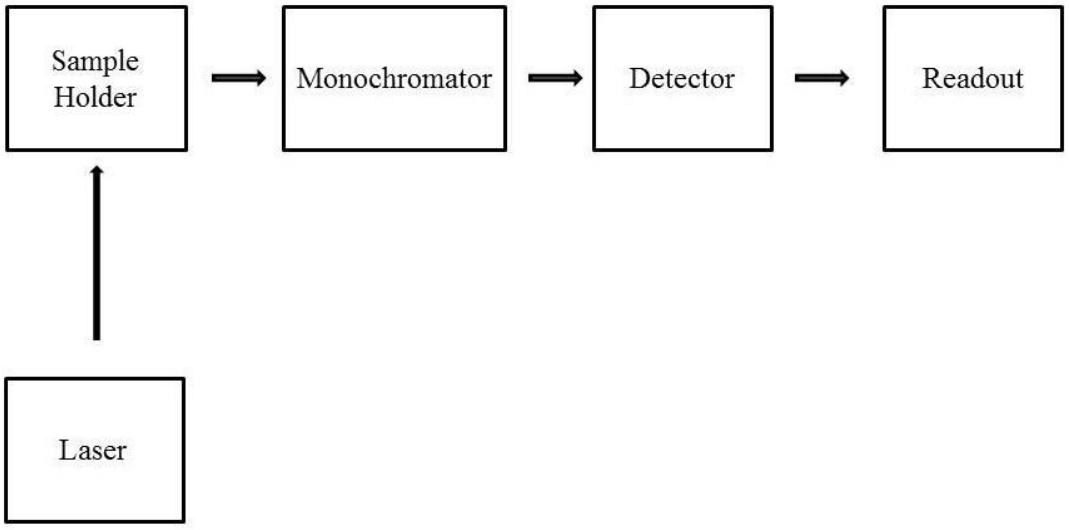

Figure 3.2.1: Box diagram of a Raman experiment

Light sources for Raman spectroscopy are lasers, with the laser in this experiment being a Krypton/Argon ion laser. Lasers are optimal for Raman spectroscopy due to the power and intensity of lasers. Additionally, lasers produce monochromatic light which is

another characteristic needed for light sources in Raman spectroscopy. The advent and use of lasers caused a dramatic increase in the applications of Raman spectroscopy due to improved intensity of signal as improvement of the signal to noise ratio.[16] Lasers rely very heavily on the principle of stimulated emission, discussed previously in this introduction. Light emitted via stimulated emission is coherent and in phase, with a low divergence of the resulting beam. In a laser, stimulated emission will dominate over absorption only when there is a population inversion. A population inversion occurs when a higher energy state has a greater population than a lower energy state. In ion lasers, an external electrical source excites the gas phase ions present in the laser to a higher energy level, with another component called the optical resonator ensuring that stimulated emission occurs. The result of this process is coherent, monochromatic light that can be used as an excitation source.[18] In krypton/argon lasers, light of many different wavelengths is produced by the stimulated emission process of the krypton and argon ions. The laser can be tuned to emit only the particular wavelength needed as an excitation source.[16] Also necessary are a laser line filter and a half-wave plate; these components lie in the path of the laser. The laser-line filter removes any wavelengths other than the wavelength of the laser line, while the half-wave plate rotates the polarization of the light from horizontal to vertical.

In the setup used in this experiment, a dispersive monochromator with a double grating is used. A grating is based on the principle of diffraction of reflected light. A grating is a highly polished surface with a large number of parallel spaced grooves covering the surface. When incident light hits the grating, it is diffracted and interference results in separation of only one wavelength of light which can be projected onto the

detector after passing through an exit slit. As the instrument scans, the grating turns so that different wavelengths are projected onto the detector as the scan occurs, which produces a spectrum.[16] Shown below in Figure 3.2.2 is a schematic of a dispersive monochromator that includes a grating.

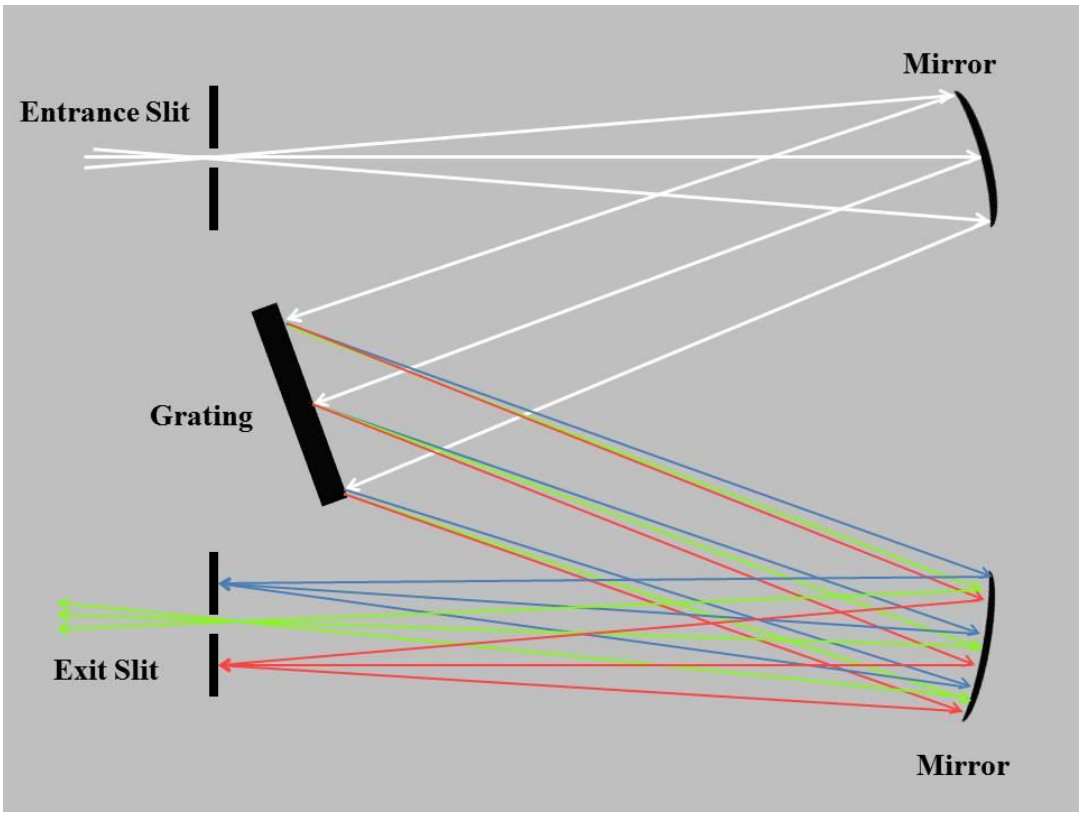

Figure 3.2.2: Schematic of a Dispersive Monochromator

The detector used in the Raman spectrometer in this experiment is a photomultiplier tube. A photomultiplier tube consists of a sealed transparent glass or quartz envelope that contains a photoemissive cathode, and anode, and several dynodes. The photomissive cathode is a piece of metal covered with either a mixture of elements or an alkali metal. When the photoemissive cathode is hit with an incident photon, electrons are released. These electrons are attracted to the dynodes in the system. The

emitted electrons strike the next dynode which release more electrons. These electrons are then attracted to the next dynode in the tube which then leads to more electrons being emitted. The result is the amplification of the original electrons emitted by the photoemissive cathode. The eventual amplification of the original photon can be as many as 10^9 electrons per photon. The amplified electrons eventually strike the anode, which records the number of electrons as a measure of the intensity of the incident light. Photomultiplier tubes are extremely sensitive to ultraviolet and visible light, so care must be taken to avoid exposure. Exposure to this light could result in irreversible damage to the detector.[16]

There are two methods of analysis used in our lab that were utilized in this study, micro-Raman spectroscopy and macro-Raman spectroscopy. In our lab, micro-Raman spectroscopy is utilized in analysis of solid samples. In micro-Raman, monochromatic, polarized laser light of narrow line width is, after passing through a laser line filter, passed through a microscope objective. The objective of the microscope allows the laser light to be focused on a very small area of the sample being analyzed. In macro-Raman, samples are examined in the bulk phase. The polarized, monochromatic, laser light passes through the sample without being focused onto a small area. Organic and aqueous liquids are easily analyzed using macro-Raman. Samples can be placed directly into the laser path in a cuvette or other holding cell.[25]

Chapter 4: Raman Spectroscopic Analysis of Halogen Containing Heterocyclic Compounds and Pyrimidine

4.1 Methods

4.1.1 Experimental Methods

A strong excitation source was used in this experiment due to the fact that Raman scattering is so much weaker than Rayleigh scattering. During this research, the 514.5 nm laser line of a SpectraPhysics Kr^+/Ar^+ laser was used as an excitation source. This same excitation source was used for obtaining all Raman spectra. Prior to the excitation source contacting the sample, two components were placed in the path of the laser in order to prepare it for contact with the sample. First, a 514.5 nm laser line filter was placed in the path of the laser to remove other wavelengths of light present in the laser line, as well as to remove any wavelengths due to ambient light in the room. The next component in the path of the laser was a half-wave plate (Thorlabs) that rotated the polarization of the light from horizontal to vertical. The power of the laser line was 1 watt for all spectra obtained during this experiment. A LabView-controlled Jobin-Yvon Ramanor HG2-S Raman spectrometer was used to analyze all samples. A photomultiplier tube was used as the

detector for the setup. The scan speed for every spectrum obtained was set to 1 wavenumber per second.

Commercially obtained 99% purity pyrimidine (Sigma-Aldrich), 98% C_6H_5Br (Sigma-Aldrich), 98% C_6H_5I (Sigma-Aldrich), 98 % C_6F_5Br (Sigma-Aldrich), and 98% C_6F_5I (Sigma-Aldrich) were used in this experiment. For mixtures of C_6H_5Br with pyrimidine and C_6H_5I with pyrimidine, mole fractions of $\chi_{\text{halogen containing compound}}$ = 0.5, 0.7, and 0.9 were prepared. For mixtures of C_6F_5Br with pyrimidine and C_6F_5I with pyrimidine, mole fractions of $\chi_{\text{halogen containing compound}}$ = 0.5, 0.7, and 0.9 were also prepared. Experimental data for each compound individually was also obtained in order to compare normal modes of the neat compounds with the normal modes observed in the mixtures. Mixtures and neat compounds were analyzed in 10 mm glass cuvettes (Precision Cells). The experimental data gathered from Raman spectroscopic analysis was graphed using the IGOR Pro graphing program.

4.1.2 Computational Methods

Quantum mechanical calculations were performed on pyrimidine, C_6H_5Br, C_6H_5I, C_6F_5Br, and C_6F_5I calculations were also carried out on Py/(X) and Py/$(X)_2$ complexes of pyrimidine and the halogen containing compound, respectively. These calculations were carried out using the Gaussian 09 software package.[19] The software optimized geometries of the molecules and complexes then calculated vibrational frequencies. For all calculations, the B3LYP method was used. [21-22] For the compounds and complexes containing bromine, the 6-311++G(2df,2pd) basis set was used during the calculations.[26-

[27] For C_6H_5I, the def2-TZVPD basis set was used. For C_6F_5I, the def2-TZVPD basis set was used for all atoms except for fluorine, with which def2-TZVP was used .[26-27] A computer program written using National Instruments LabView was used to view the theoretical data. As the data is computed in intensity values, the theoretical spectra do not have the broad peaks that are observed experimentally. This program overlays Lorentzian functions over the narrow peaks in order to broaden them, resulting in a spectrum that is more easily comparable to experimental spectra.

4.2 Experimental and Theoretical Shifts for all Mixtures

Included in this section are all of the experimental and theoretical shifts of pyrimidine's normal modes of the complexes that were studied, which will be referenced in later sections. In this study, the perturbations in the normal modes on the Lewis base, nitrogen in pyrimidine, are studied. This is unique when it comes to the study of halogen bonding interactions, as the majority of previous studies have involved concentrating on the perturbations of the carbon-halogen bond. This new focus will provide new information to the scientific community regarding halogen bonding interactions. Shown below in Figure 4.2.1 are the experimental shifts of pyrimidine's normal modes in the four mixtures analyzed experimentally.

Table 4.2.1: Experimental Shifts of Pyrimidine's Normal Modes (cm^{-1})

Mode	Py	With C_6H_5Br	With C_6H_5I	With C_6F_5Br	With C_6F_5I
ν_{16b}	350	0	-3	0	0
ν_{16a}	401	-2	-1	0	0
ν_{6b}	626	-1	-1	0	+1
ν_{6a}	681	-1	0	0	0
ν_{1}	990	-2	-2	0	+5
$\nu_{10b}+\nu_{16b}/\nu_{12}$	1055	-3	-4	-1	0
$\nu_{10b}+\nu_{16b}/\nu_{12}$	1076	0	-3	0	0
ν_{9a}	1139	0	-1	+1	+2
ν_{15}	1159	0	0	0	0
ν_{3}	1228	0	-5	-3	-4
ν_{8a}	1564	-1	0	0	+3
ν_{8b}	1565	0	0	0	+6

These experimental shifts will be discussed in detail in the following sections of this chapter that focus on each experiment individually. In addition to experimental shifts, theoretical shifts were also determined in order to compare experimental results to those observed experimentally. Shown below in Table 4.2.2 are the theoretical shifts in pyrimidine's normal modes with the bromine containing complexes that were analyzed.

Table 4.2.2: Theoretical Shifts of Pyrimidine's Normal Modes with Bromine Containing Complexes $(cm^{-1})^2$

Mode	Py/C_6H_5Br	Py/$(C_6H_5Br)_2$	Py/C_6F_5Br	Py/$(C_6F_5Br)_2$
ν_{16b}	0	+2	+2	+4
ν_{16a}	+2	+4	+2	+4
ν_{6b}	+2	+3	+3	+5
ν_{6a}	0	+1	0	+1
ν_{1}	+2	+3	+3	+5
ν_{9a}	+1	+1	0	0
ν_{15}	+1	+1	0	+2
ν_{3}	+1	+1	+1	+1
ν_{8a}	+2	+3	0	+3
ν_{8b}	0	0	+3	+3

The theoretical shifts for iodine containing molecular complexes were also determined. Shown below in Table 4.2.3 are the theoretical shifts in pyrimidine's normal modes with the iodine containing complexes that were analyzed.

[2] B3LYP/6-311++G(2df,2pd)

Table 4.2.3: Theoretical Shifts of Pyrimidine's Normal Modes with Iodine Containing Complexes (cm^{-1})

Mode	Py/C_6H_5I[3]	$Py/(C_6H_5I)_2$[4]	Py/C_6F_5I[5]
ν_{16b}	+2	+4	+4
ν_{16a}	+2	+4	+5
ν_{6b}	+3	+5	+5
ν_{6a}	0	+1	+1
ν_{1}	+3	+5	+6
ν_{9a}	0	0	0
ν_{15}	0	+2	+2
ν_{3}	+1	+1	+2
ν_{8a}	0	+3	-1
ν_{8b}	+3	+3	7

These theoretical shifts will be discussed in detail in sections of this chapter following this section that focus on the individual experiments.

In addition to determining theoretical shifts, theoretical calculations were also used to determine the binding energies of the complexes that were analyzed. These binding energies are shown below in Table 4.2.4

[3] B3LYP/def2-TZVPD
[4] B3LYP/def2-TZVPD
[5] B3LYP/def2-TZVPD Fluorine def2-TZVP

Table 4.2.4: Binding Energies of Theoretical Complexes

Complex	Binding Energy (kcal/mol)
Py/C_6H_5Br	-0.72
Py/$(C_6H_5Br)_2$	-1.52
Py/C_6F_5Br	-2.57
Py/$(C_6F_5Br)_2$	-4.93
Py/C_6H_5I	-1.69
Py/$(C_5H_5I)_2$	-3.30
Py/C_6F_5I	-3.48

These binding energies shed light on the magnitude of the interaction that is occurring in this theoretical complex. These binding energies will be discussed later in the sections of this chapter.

Before beginning discussion of these results, the reason why C_6H_5Cl and C_6F_5Cl were not analyzed must be addressed. These two molecules would have the smallest σ-hole due to the halogen bonding theory that is discussed in Chapter 1. Additionally, in the theoretical electrostatic potential map shown in Figure 1.2.1, C_6F_5Cl has the smallest σ-hole. The small magnitude of this hole suggests that no halogen bonding interactions will occur, and therefore experimental analysis of these molecules would not give any useful information.

4.3 Analysis of C_6H_5Br and Pyrimidine

Mixtures of C_6H_5Br and pyrimidine at χ_{C6H5Br} = 0.5, 0.7, and 0.9 were analyzed to determine if perturbations in pyrimidines normal modes would be observed due to halogen bonding interactions between bromine on C_6H_5Br and nitrogen on pyrimidine. As discussed in Chapter 1 of this thesis, the strength of halogen bonding interactions increased from fluorine<chlorine<bromine<iodine. Additionally, it was discussed that highly electron withdrawing groups present on the halogen containing molecule could increase the size of the positive σ-hole present on the halogen. C_6H_5Br contains bromine, a weaker halogen bonding atom than iodine, and does not have any highly electron withdrawing groups present on the molecule. Therefore, the size of the positive region of electrostatic potential on bromine was postulated to be quite small in magnitude. This means that a halogen bond interaction between bromine on C_6H_5Br and nitrogen on pyrimidine was not likely to form due to halogen bond theory. The experimental data gathered from Raman spectroscopic analysis was graphed using the IGOR Pro graphing program in order to determine if any observable spectral changes had occurred due to interactions between C_6H_5Br and pyrimidine. Specifically, changes in position of pyrimidine's normal modes were looked for, as this would indicate an interaction between pyrimidine and C_6H_5Br. Experimental shifts in these normal modes of pyrimidine were determined by comparing the position of the pyrimidine normal mode in the spectrum of neat pyrimidine with the position of the same normal mode in the highest mole fraction solution of C_6H_5Br. The experimental Raman spectra are shown below in Figure 4.3.1.

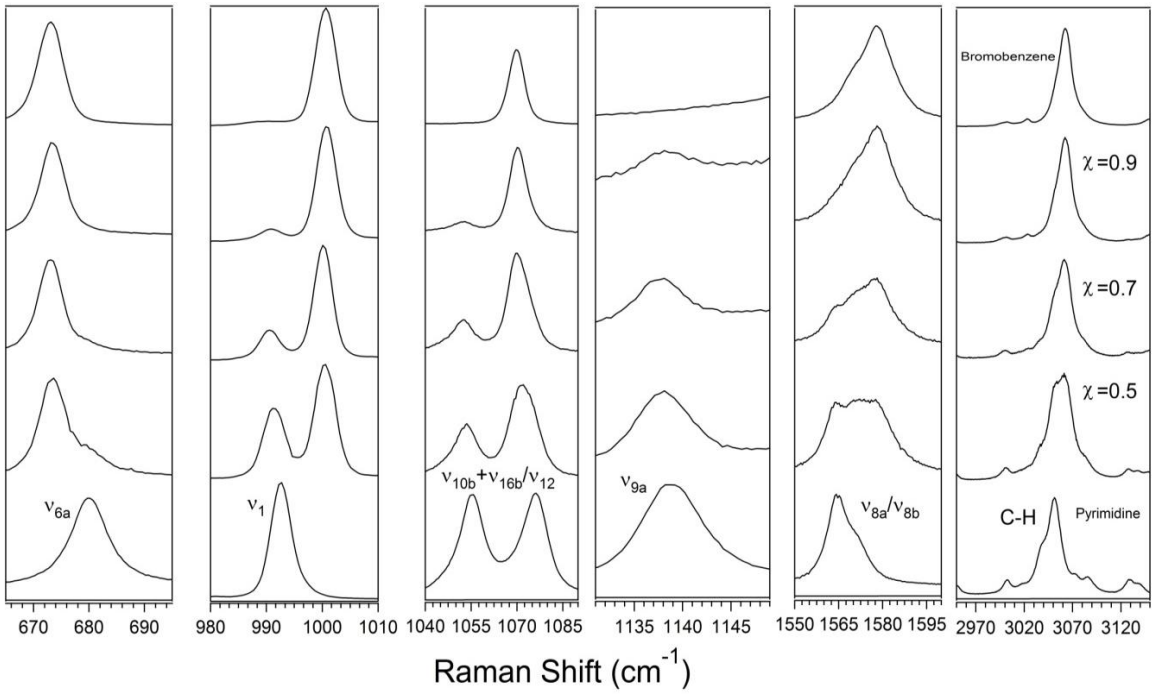

Figure 4.3.1: Experimental Spectra of C_6H_5Br Pyrimidine Mixtures

When analyzing the experimental data, as can be seen in the Raman spectra, there were vibrational modes of C_6H_5Br that overlapped with the pyrimidine normal modes that were analyzed. This made determining exact values of shifts difficult due to the overlap. The experimental shifts observed are shown in section 4.2 in Table 4.2.1. As shown in Table 4.2.1, there were few spectral changes observed, with the changes that were observed being very small. In addition, the shifts observed were all red shifts, which indicate a shift to lower energy. A shift to lower energy would not be expected with halogen bonding interactions, as previous studies involving pyrimidine hydrogen bonding interactions involved a blue shift to higher energy of pyrimidine's normal modes due to hydrogen bonding.[24] As discussed in Chapter 1, halogen bonding and hydrogen bonding are analogous in many ways, and so a red shift in pyrimidines normal modes suggest that interactions occurring are not due to halogen bonding.

Theoretical calculations at the B3LYP level of method using the 6-311++G(2df,2pd) basis set were also carried out on complexes involving pyrimidine and C_6H_5Br. The optimized structures are shown below in Figure 4.3.2 and 4.3.3.

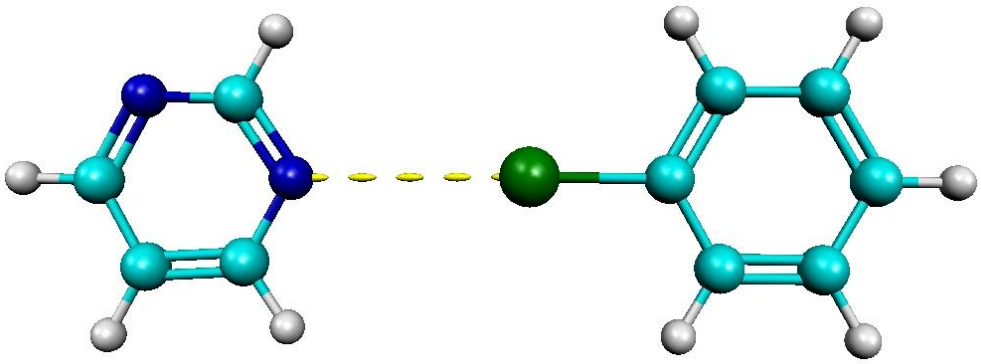

Figure 4.3.2: Optimized Structure of Py/ C_6H_5Br

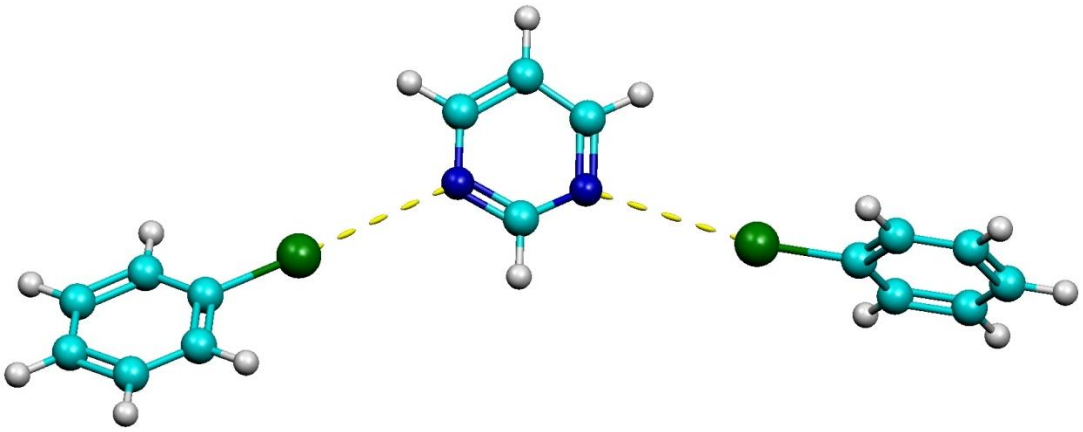

Figure 4.3.3: Optimized Structure of Py/ $(C_6H_5Br)_2$

The pyrimidine normal modes that were examined experimentally were also examined theoretically. The theoretical shift values for the pyrimidine normal modes of interest are shown in section 4.2 in Table 4.2.2. The modes $\nu_{10b} + \nu_{16b}$ / ν_{12} that are examined experimentally are not observed in the theoretical calculations, as they are a Fermi resonance. As Fermi resonance occurs when two vibrational modes close in energy have

the same symmetry, and therefore they combine with each other to form a combination of the two modes.[17] This phenomenon is not accounted for during quantum mechanical calculations. The theoretical shifts observed differ from what was observed experimentally. The optimized complex containing two C_6H_5Br molecules and one pyrimidine molecule is not at all similar to what was observed experimentally; it has large blue shift values which are larger in magnitude than anything observed experimentally. The complex with one C_6H_5Br and one pyrimidine is the most similar to what was observed experimentally, with modes ν_{16b} and ν_{8b} matching the observed experimental shift of zero wavenumbers. The other theoretical shifts in this complex were blue shifts small in magnitude, unlike the small red shifts observed experimentally.

The theoretical binding energies of these two complexes are shown in Table 4.2.4, and correspond to the strength of the interaction occurring. As shown in the table, the relative binding energies of the complexes are low at -0.72 and -1.52 kilocalories per mole for Py/C_6H_5Br and Py/($C_6H_5Br)_2$, respectively. This small binding energy, when compared to hydrogen bonding energies which can range from -4 to -10 kilocalories per mole, suggests that there is not a significant halogen bonding interaction that could occur experimentally.[2]

This theoretical and experimental data suggests that experimentally, there were no significant halogen bonding interactions between C_6H_5Br and pyrimidine in solution.

4.4 Analysis of C_6H_5I and Pyrimidine

Mixtures of C_6H_5I and pyrimidine at χ_{C6H5I} = 0.5, 0.7, and 0.9 were analyzed to determine if perturbations in pyrimidines normal modes would be observed due to halogen bonding interactions between iodine on C_6H_5I and nitrogen on pyrimidine. As mentioned previously, iodine has the potential to form the strongest halogen bond interactions due to it having the potential to form the largest σ-hole on the halogen atom. As discussed previously, the magnitude of this σ-hole could be increased by having highly electron-withdrawing atoms on the benzene ring, as these help to increase the size of the σ-hole on the halogen. C_6H_5I does not have any electron withdrawing groups present, but it should have a σ-hole larger in magnitude than the one present on C_6H_5Br. It was hypothesized that more noticeable perturbations to pyrimidines normal modes would be observed experimentally in mixtures of C_6H_5I and pyrimidine. However, it is still likely that any changes observed experimentally will be small, as C_6H_5I does not have any highly electron withdrawing groups present to increase the magnitude of the σ-hole. Shown below in Figure 4.4.1 are the experimental Raman spectra of these mixtures.

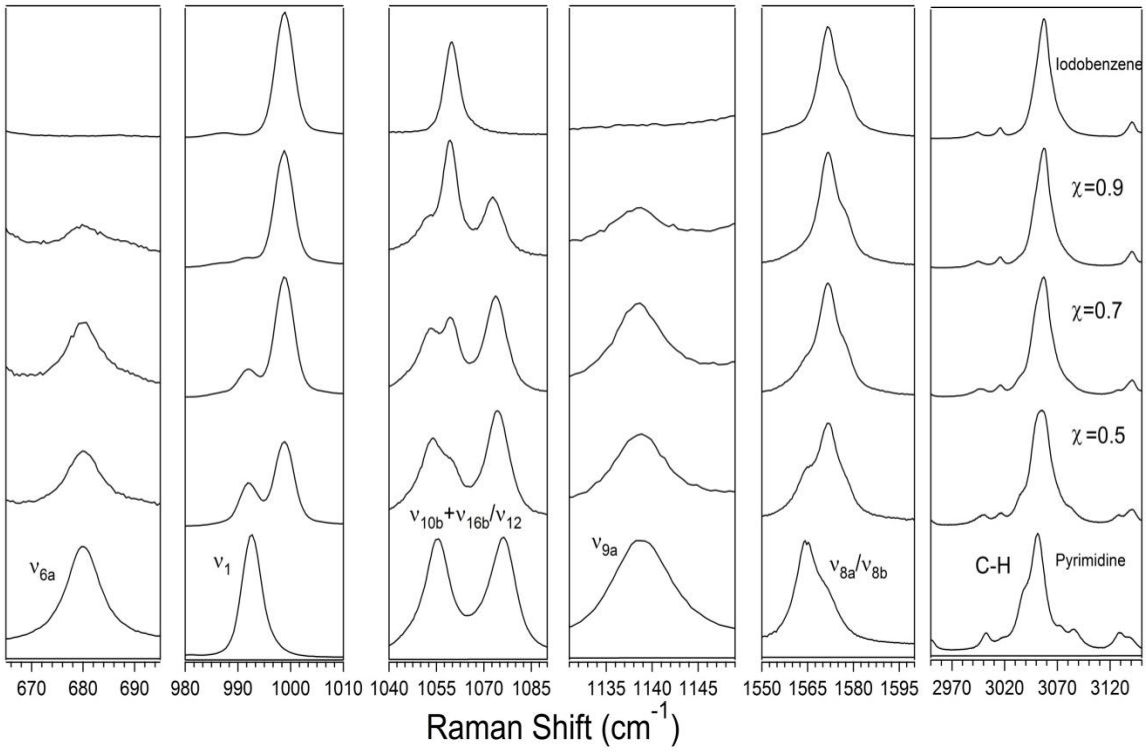

Figure 4.4.1: Experimental Spectra of C_6H_5I Pyrimidine Mixtures

As in C_6H_5Br, there are modes of C_6H_5I that overlap with the modes of pyrimidine that were analyzed. This made determining exact experimental shifts difficult due to the C_6H_5I modes masking the modes of pyrimidine at higher concentrations of C_6H_5I. Shown in section 4.2 in Table 4.2.1 are the shifts observed in the normal modes of pyrimidine in this mixture. As shown in Table 4.2.1, experimental shifts observed were all red shifts, or a shift to lower energy. This is similar to what was observed in mixtures of C_6H_5Br and pyrimidine. The shift to lower energy of the normal modes of pyrimidine suggests that there are not halogen bond interactions occurring between C_6H_5I and pyrimidine, as previous studies involving hydrogen bond interactions between pyrimidine and water resulted in blue shifts of pyrimidine's normal modes.

Theoretical calculations at the B3LYP level of method using the def2-TZVPD basis set were also carried out on complexes involving pyrimidine and C_6H_5I. The basis set employed for calculations involving bromine, 6-311++G(2df,2pd), does not contain basis functions corresponding to the iodine atom. Because of this, a basis set containing functions for the iodine atom had to be found. Though there are many basis sets that contain iodine as well as the remaining atoms in the complex, one had to be found that proved to be reliable in predicting shifts due to noncovalent interactions such as hydrogen bonding and halogen bonding. Another student in the Hammer lab, Katelyn Allen, performed a theoretical analysis of pyrimidine water clusters using the basis sets def2-SVP, def2-SVPD, def2-TZVP, def2-TZVPD, def2-TZVPP, def2-TZVPPD, def2-QZVP, def2-QZVPD. Def2-QZVPP, and def2-QZVPPD. This analysis was compared to previous calculations by student Austin Howard on pyrimidine water clusters that used the 6-311++G(2df, 2pd) basis set.[24] This analysis was done in order to determine which of the def2 basis sets most accurately predicted the shifts due to noncovalent interactions observed using the 6-311++G(2df, 2pd) basis set. The basis set that most accurately predicted these interactions was the def2-TZVPD basis set, which was then used for analysis of complexes containing iodine.[26-27] The optimized structures are shown below in Figure 4.4.2 and 4.4.3.

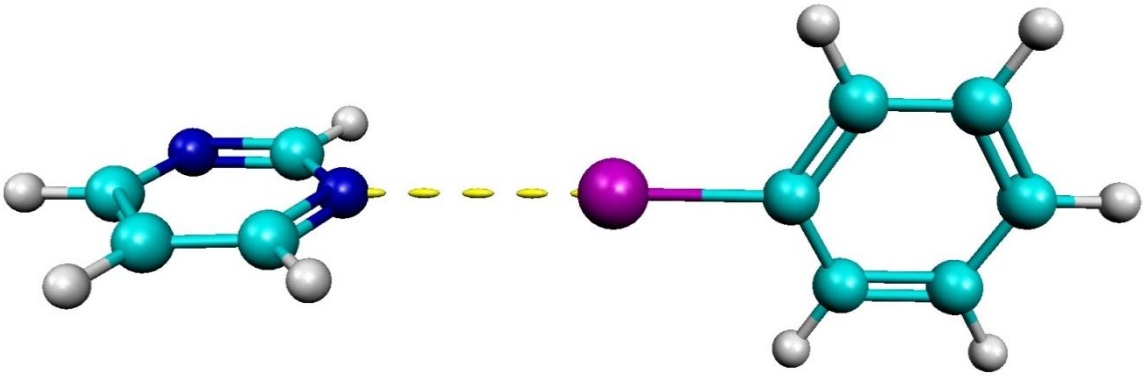

Figure 4.4.2: Optimized Structure of Py/C_6H_5I

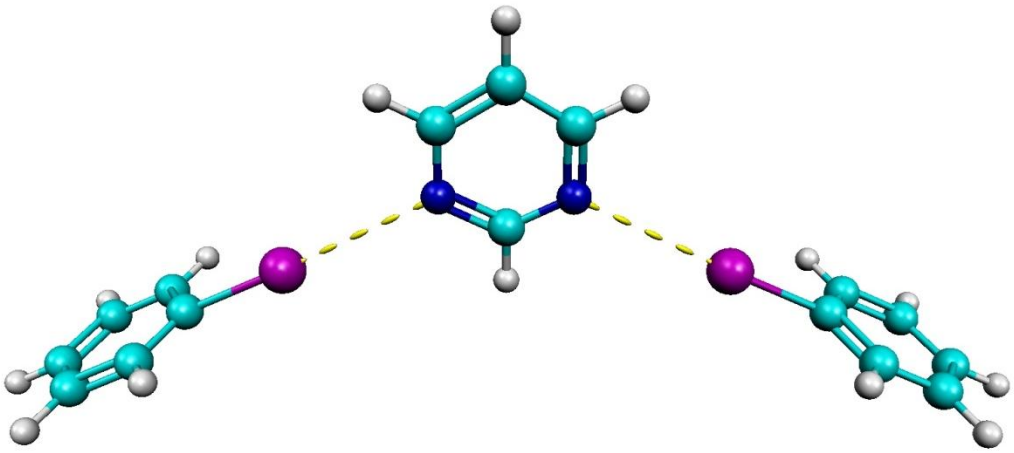

Figure 4.4.3: Optimized Structure of Py/$(C_6H_5I)_2$

The pyrimidine normal modes that were examined experimentally were also examined theoretically. The theoretical shift values for the pyrimidine normal modes of interest are shown in section 4.2 in Table 4.2.3. The shifts observed in theoretical calculations differ from what was observed experimentally. The complex of two C_6H_5I molecules with pyrimidine differed significantly from the shifts observed experimentally. In this theoretical complex, large blue shifts were observed in pyrimidine's normal modes. In the theoretical complex of one C_6H_5I and pyrimidine, blue shifts were predicted in the modes where red shifts were observed experimentally. However, in modes ν_{6a} , ν_{15} , and ν_{8a}

there were no shifts observed both theoretically and experimentally, which suggests that this complex agrees best with what was observed experimentally. The relative binding energies of these theoretical complexes are shown in table 4.2.4. These binding energies were -1.69 and -3.30 kilocalories per mole for Py/C_6H_5I and Py/($C_6H_5I)_2$, respectively. Though these values are larger than the values observed for the corresponding bromine containing complex, they are still smaller in magnitude than binding energies of hydrogen bonds. This information coupled with the red shifts observed experimentally, led to the conclusion that no significant halogen bonding interactions are occurring between pyrimidine and C_6H_5I in experiment.

4.5 Analysis of C_6F_5Br and Pyrimidine

Mixtures of C_6F_5Br and pyrimidine at χ_{C6F5Br}= 0.5, 0.7, and 0.9 were analyzed to determine if perturbations in pyrimidines normal modes would be observed due to halogen bonding interactions between bromine on C_6F_5Br and nitrogen on pyrimidine. The molecule C_6F_5Br contains five fluorine atoms, which are highly electron withdrawing. These fluorine atoms in theory pull electron density away from the bromine atom, increasing the size of the positive σ-hole present on bromine. A larger σ-hole increases the likelihood that there will be an interaction between nitrogen on pyrimidine and the σ-hole present on C_6F_5Br. Though the fluorine atoms will increase the size of the σ-hole present on bromine, bromine does not have the potential to form the strongest halogen bond interactions. Therefore, C_6F_5Br should theoretically contain a larger σ-hole than C_6H_5Br, but it will not have a σ-hole as large as its iodine counterpart, C_6F_5I. It was hypothesized that experimental changes in pyrimidine's normal modes would be affected

more by C_6F_5Br then they were affected by C_6H_5Br and C_6H_5I. Shown below in Figure 4.5.1 are the experimental Raman spectra of the mixtures.

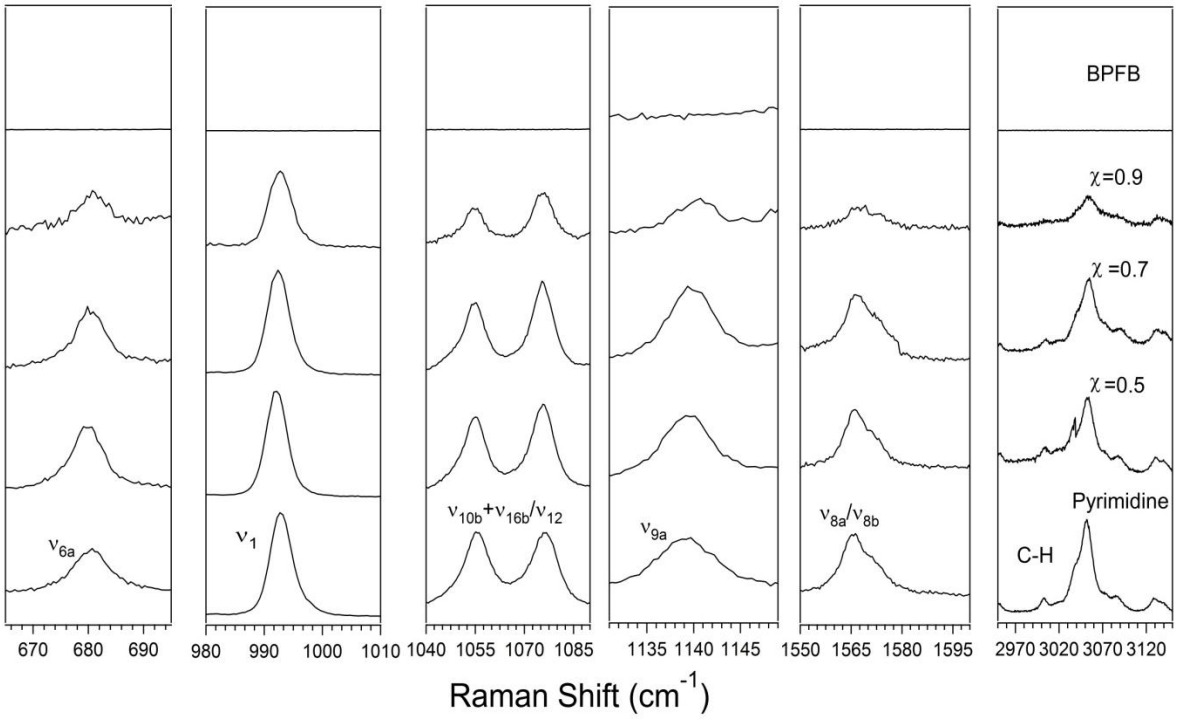

Figure 4.5.1: Experimental Spectra of C_6F_5Br (BPFB) Pyrimidine Mixtures

Unlike in experiments involving C_6H_5Br and C_6H_5I, there were no modes of C_6F_5Br present that overlapped with the modes of pyrimidine that were analyzed. This made determining the experimental shifts of the pyrimidine modes analyzed easier than in the previous experimental mixtures. Shown in section 4.2 in Table 4.2.1 are the experimental shifts in pyrimidine's normal modes that were observed. As shown in Table 4.2.1, only three shifts in the modes of pyrimidine analyzed were observed experimentally. These occurred in modes $\nu_{10b}+\nu_{16b}/\nu_{12}$, ν_{9a}, and ν_3. There were more shifts observed experimentally in C_6H_5Br and C_6H_5I, however these shifts were all red shifts to lower energy. One of the modes, ν_{9a}, exhibited a blue shift, or a shift to higher energy. This is

the first instance during the experiments that a blue shift was observed experimentally. However, this shift of one wavenumber is so small in magnitude that it is difficult to directly attribute it to halogen bond interactions between pyrimidine and C_6F_5Br. The other two shifts observed were red shifts also small in magnitude, similar to what was observed experimentally in mixtures of C_6H_5Br and C_6H_5I with pyrimidine. This analysis indicates that it is not likely halogen bond interactions occurred between C_6F_5Br and pyrimidine.

Theoretical calculations at the B3LYP level of method using the 6-311++G(2df,2pd) basis set were also carried out on complexes involving pyrimidine and C_6F_5Br. The optimized structures are shown below in Figure 4.5.2 and 4.5.3

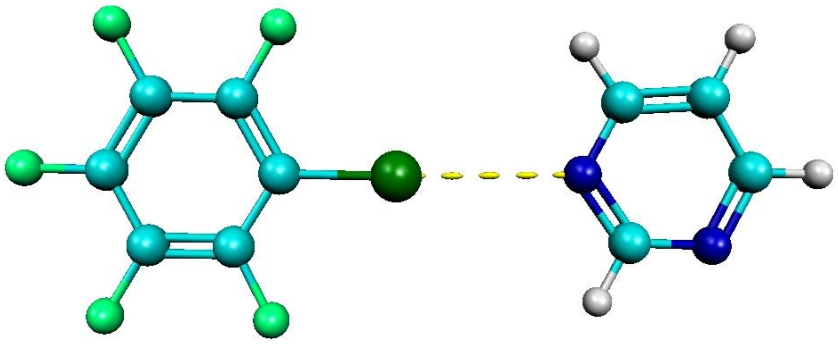

Figure 4.5.2: Optimized Structure of Py/C_6F_5Br

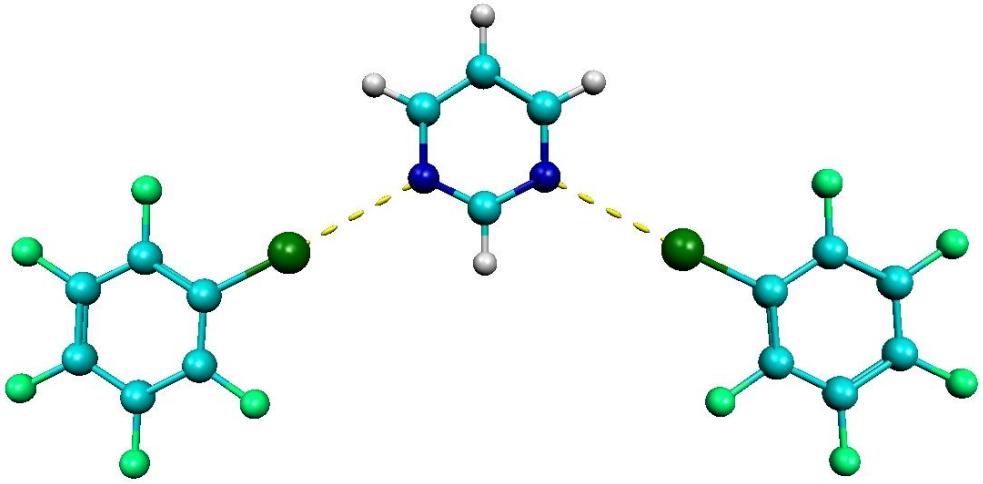

Figure 4.5.3: Optimized Structure of Py/(C_6F_5Br)$_2$

The pyrimidine normal modes that were examined experimentally were also examined theoretically. The theoretical shift values for the pyrimidine normal modes of interest are shown in section 4.2 in Table 4.2.2. Theoretical calculations involving C_6F_5Br and pyrimidine resulted in all blue shifts. The two C_6F_5Br pyrimidine complex theoretical results did not at all match what was observed experimentally. This indicates that it is not likely two C_6F_5Br are interacting with one pyrimidine molecule simultaneously in solution. The theoretical results for the one C_6F_5Br pyrimidine complex had results closer to what was observed experimentally. In modes ν_{6a}, ν_{15}, and ν_{8a} there were no shifts observed both theoretically and experimentally, which suggests that this complex agrees best with what was observed experimentally. Binding energies for these theoretical complexes were also determined. These binding energies are show in Table 4.2.4 and are -2.57 and -4.93 kilocalories per mole for Py/C_6F_5Br and Py/($C_6F_5Br)_2$, respectively. These binding energies are great than those observed in the non-fluorinated bromine and iodine containing complexes, which is expected as the introduction of a highly electron withdrawing atom such as fluorine increases the size of the σ-hole present. The binding

energy of the Py/($C_6F_5Br)_2$ complex competes with the values of binding energies that are observed in hydrogen bonded complexes. Despite this theoretical evidence of an interaction occurring, experiment clearly shows that a non-covalent interaction did not occur. The small value of the blue shift observed experimentally as well as the lack of blue shifts in the pyrimidine modes analyzed suggests that no significant halogen bond interactions occurred experimentally, even though in theory C_6F_5Br would have a larger σ-hole than C_6H_5Br or C_6H_5I.

4.6 Analysis of C_6F_5I and Pyrimidine

Mixtures of C_6F_5I and pyrimidine at χ_{C6F5I}= 0.5, 0.7, and 0.9 were analyzed to determine if perturbations in pyrimidines normal modes would be observed due to halogen bonding interactions between iodine on C_6F_5I and nitrogen on pyrimidine. Like C_6F_5Br, C_6F_5I should in theory have a larger σ-hole due to the fluorine atoms present on the molecule. Additionally, iodine inherently has the potential to form the largest σ-hole. C_6F_5I should in theory have the largest σ-hole of any of the bromine and iodine containing molecules that were analyzed in this series of experiments. Therefore, it was anticipated that this experiment would have the greatest potential to affect the normal modes of pyrimidine due to halogen bonding interactions. Shown below in Figure 4.6.1 are the experimental Raman spectra.

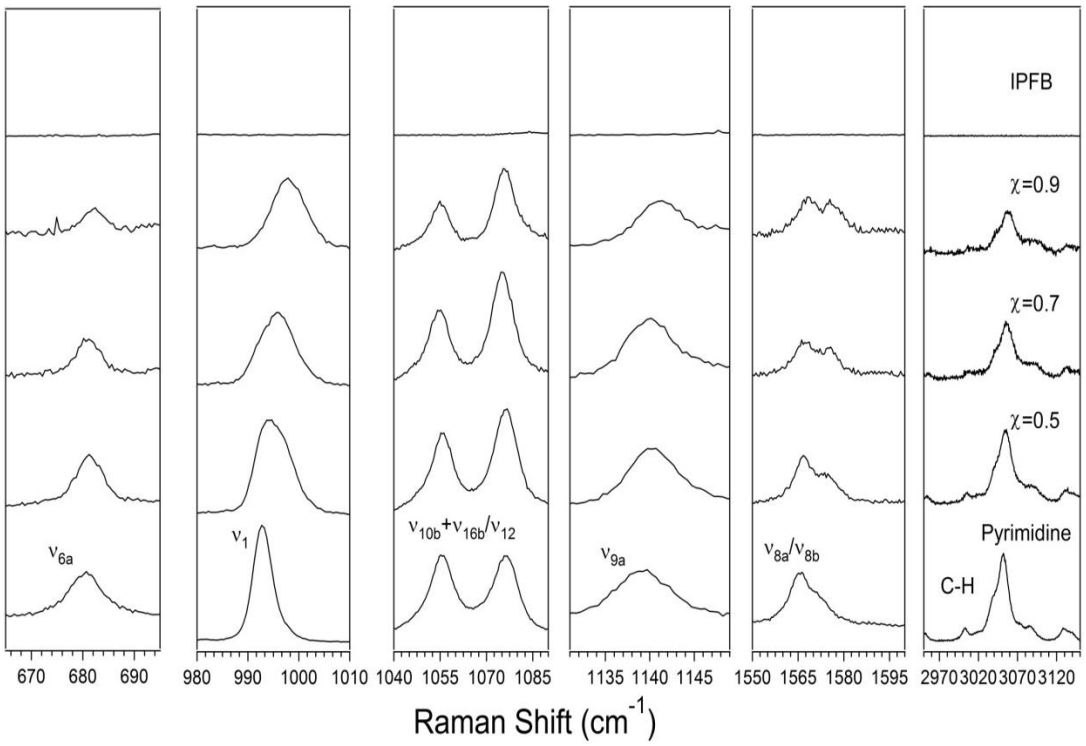

Figure 4.6.1: Experimental Spectra of C_6F_5I (IPFB) Pyrimidine Mixtures

It can be easily seen in these spectra that blue shifts in pyrimidine's normal modes are occurring. C_6F_5I, like C_6F_5Br, does not have any normal modes that overlap with the normal modes of pyrimidine that were analyzed. This easily allowed determination of the experimental shift values. Shown in section 4.2 in Table 4.2.1 are the experimental shifts observed in mixtures of C_6F_5I and pyrimidine. As shown in Table 4.2.1, there were shifts observed in six of pyrimidine's normal modes. Modes v_{6b}, v_1, v_{9a}, $v_{8a,}$ and v_{8b} all exhibited blue shifts experimentally. This is similar to what was observed in a previous study involving hydrogen bonding and pyrimidine. The same modes in the hydrogen bonding study exhibited blue shifts experimentally, which suggests that a similar interaction is occurring in the solution of pyrimidine and C_6F_5I. The shifts in pyrimidine's normal modes from this study are shown below in Table 4.6.1below.

Table 4.6.1: Experimental Shifts of Pyrimidine's Normal Modes in a Water/Pyrimidine Mixture[24]

Mode	Pyrimidine Original	With Water
ν_{16b}	350	+2
ν_{16a}	401	+2
ν_{6b}	626	+13
ν_{6a}	681	+5
ν_{1}	990	+14
ν_{9a}	1139	+5
ν_{15}	1159	+9
ν_{3}	1228	+3
ν_{8a}	1564	+6
ν_{8b}	1565	+12

As shown in Table 4.6.1 above, in the hydrogen bonding study, the shifts were slightly larger in magnitude, which suggests that the interaction occurring in this experiment is not as strong. However, the presence of blue shifts in the mixture of pyrimidine and C_6F_5I is an indication that a similar noncovalent interaction is occurring. These shifts suggest that a halogen bonding interaction could be occurring between pyrimidine and C_6F_5I. This was not observed in the experiments involving C_6H_5Br, C_6H_5I, and C_6F_5Br. This makes sense, as C_6F_5I in theory has the largest σ-hole and therefore the greatest potential to participate in halogen bonding interactions with pyrimidine.

Theoretical calculations at the B3LYP level of method using the def2-TZVPD basis set with the diffuse fluorine functions removed were carried out on complexes involving pyrimidine and C_6F_5I. The diffuse functions for fluorine were removed from the def2-TZVPD basis set for these calculations due to linear dependencies when the

diffuse fluorine functions were included. The optimized structure of pyrimidine and C_6F_5I is shown below in Figure 4.6.2.

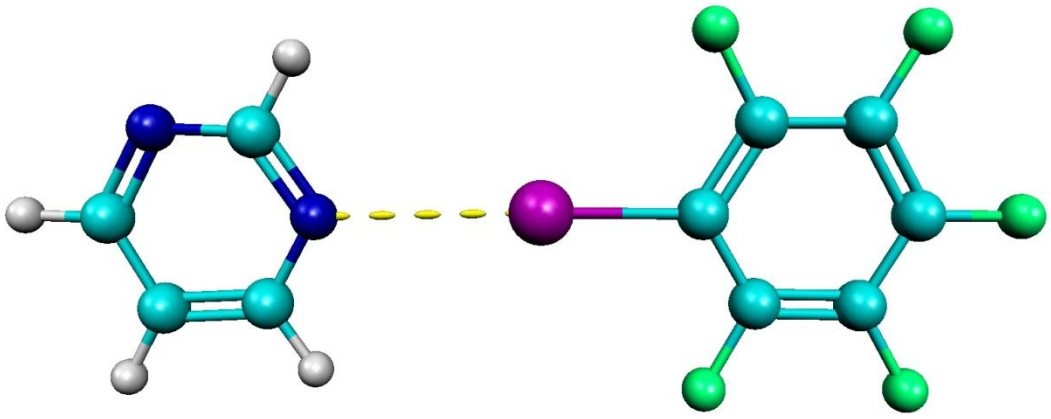

Figure 4.6.2: Optimized Structure of Py/C_6F_5I

The pyrimidine normal modes that were examined experimentally were also examined theoretically. Calculations involving two C_6F_5I molecules and pyrimidine are currently on going. The theoretical shift values for the pyrimidine normal modes of interest are shown in section 4.2 in Table 4.2.3. Theoretical calculations involving C_6F_5I and pyrimidine resulted in blue shifts with one small red shift present in ν_{8a}. The results for the one C_6F_5I pyrimidine complex matched well with what was observed experimentally. Experimentally, blue shifts were observed in modes ν_{6b}, ν_1, ν_{9a}, ν_{8a}, and ν_{8b} . Of these five modes, ν_{6b}, ν_1, and ν_{8a} also exhibited blue shifts theoretically. The theoretical shift values for ν_1 and ν_{8a}, 6 cm^{-1} and 7 cm^{-1}, respectively, matched very well with the values of 5 cm^{-1} and 6 cm^{-1} that were observed experimentally. This match with experiment suggests that the theoretical calculations carried out were accurate in predicting the results of the interaction between C_6F_5I and pyrimidine. The binding energy of this theoretical complex is shown in Table 4.2.4 and was determined to be -3.48 kilocalories per mole. This value

is only slightly smaller than those observed for hydrogen bonded complexes. A previous theoretical study involving fluorinated iodine containing complexes found the highest binding energy to be -5.8 kilocalories per mole, which occurred due to an interaction between NH_3 and CF_3I.[8] This value is encouraging for our theoretical studies, as though it is larger, it does show that similar binding energies have been observed in known halogen bonded complexes. As the theoretical calculation for the Py/C_6F_5I agrees with experiment, it is postulated that an interaction similar in energy to -3.48 kilocalories per mole is occurring experimentally.

Though calculations with two C_6F_5I and pyrimidine are ongoing, it is predicted that the most accurate theoretical prediction will come from the Py/C_6F_5I complex that has been discussed here. This is predicted due to the evidence from the C_6H_5Br, C_6H_5I, and C_6F_5Br computational studies, where for all three experiments the one to one theoretical complex was the most accurate when compared to experiment.

The large value of the blue shifts observed in experiment and successfully predicted by theory suggests that halogen bonding interactions are occurring between the C_6F_5I and pyrimidine. This agrees with halogen bonding theory, as the molecule C_6F_5I had the largest potential of all of the bromine and iodine molecules studied to participate in this interaction due to the large magnitude of the σ-hole present on the molecule.

4.7 Conclusions

Analysis of experimental data for the four mixtures yields valuable information about possible halogen bonding interactions occurring in this system. For the mixtures of C_6H_5Br and C_6H_5I with pyrimidine, there were no experimental changes that could possibly be attributed to halogen bonding. Theoretical calculations for these complexes agreed with experimental results in several modes of pyrimidine, but for the most part predicted blue shifts which were not observed experimentally. Theoretically for both C_6H_5I and C_6H_5Br, the complex involving one halogen containing molecule and pyrimidine most closely resembled what was observed experimentally. The mixture of C_6F_5Br and pyrimidine exhibited few shifts, but three of the modes did match with what was observed theoretically. However, the shifts predicted with theory were blue shifts, while experimentally two red shifts and only one small blue shift were observed. The blue shift was so small in magnitude that it is difficult to directly attribute it to halogen bonding interactions. Theoretically, the one to one complex of C_6F_5Br and pyrimidine most accurately predicted the changes that were observed experimentally. C_6F_5I mixtures were the only mixtures that exhibited shifts characteristic of a noncovalent interaction occurring between the two molecules. Significant blue shifts were observed which suggests that halogen bonding interactions are occurring between C_6F_5I and pyrimidine. Theoretical calculations of C_6F_5I and pyrimidine successfully predicted the largest blue shifts observed experimentally. This suggests that C_6F_5I and pyrimidine are participating in a halogen bonding interaction in the solutions studied in this experiment.

Chapter 5: Micro-Raman Analysis of Pyridyl-Thiophene and Halogen Bond Containing Co-Crystals

5.1 Introduction

This experiment involved characterization of co-crystals grown by Dr. Davita Watkins of the University of Mississippi and her lab students. The crystals were grown using pyridyl-thiophene and C_6F_5I. These co-crystals employ halogen bonding interactions in the structure of the crystal. The micro-Raman set up was used to analyze these crystals. The monomer, pyridyl-thiophene, was analyzed as well as the co-crystal in order to observe any spectral changes in the normal modes of pyridyl-thiophene. The 647.1 nm line of a SpectraPhysics Kr^+/Ar^+ laser was used as an excitation source. A laser line filter and half wave plate were placed in the laser line in order to remove extraneous wavelengths of light and to change the polarization of the light. The laser power was 100 milliwatts during analysis. A LabView-controlled Jobin-Yvon Ramanor HG2-S Raman spectrometer was used to analyze all samples. A photomultiplier tube was used as the detector for the setup. The solid crystals were placed onto a microscope slide and placed on the microscope stage in the path of the laser. The crystals were scanned from 20-2000

cm^{-1} four times at a speed of 2 cm^{-1} per second. The experimental data gathered from Raman spectroscopic analysis was graphed using the IGOR Pro graphing program. Theoretical calculations of pyridyl-thiophene and the co-crystal were carried out by Dr. Greg Tschumper of the University of Mississippi. The X-Ray crystal structure data was provided by Dr. Amala Dass of the University of Mississippi.

5.2 Analysis of Experimental Data and Comparison to Theory

The individual compounds, pyridyl-thiophene and the co-crystal, were analyzed individually first and compared to theory. Analysis of the experimental Raman spectra of the pyridyl-thiophene monomer was complicated by the presence of an emissive background. In order to more easily analyze the data, the background was fit to a 24^{th} degree polynomial and subtracted from the data in order to generate the final Raman spectrum. Theoretical calculations were carried out using the def2-TZVPD basis set at the M06-2X level of method.[26-28] Unlike previous calculations in this paper, the B3LYP method was not utilized because it did not adequately describe this system. Despite the poor signal to noise ratio in some regions of the spectrum, experimental data agreed very well with theoretical results. The comparison between experimental and theoretical Raman spectra is shown below in Figure 5.2.1

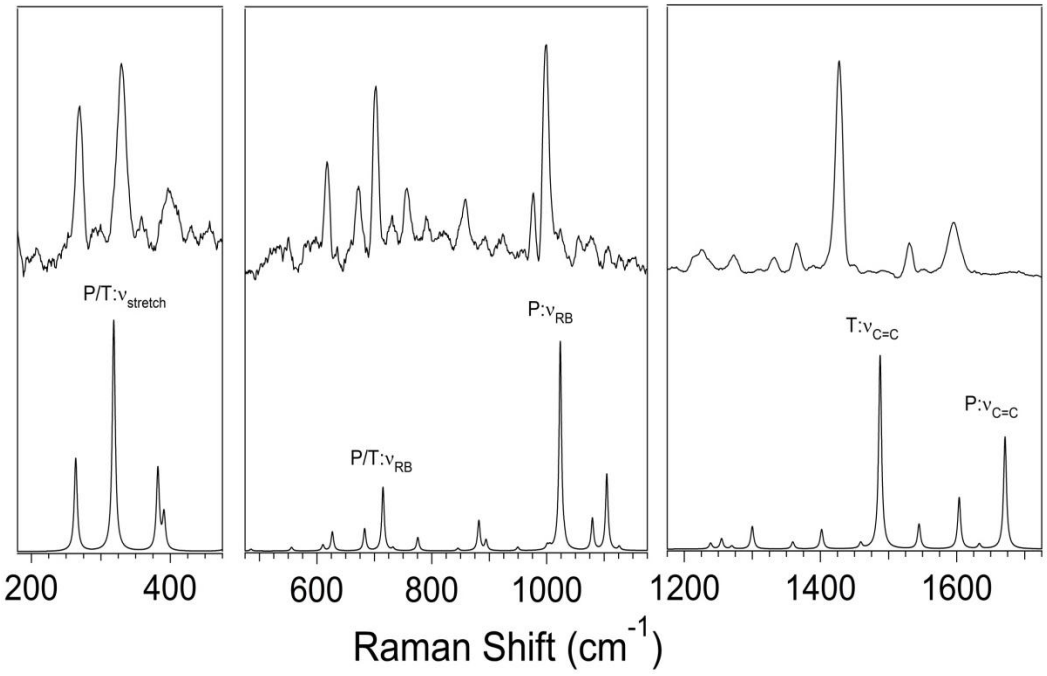

Figure 5.2.1: Comparison of Experiment to Theory of Pyridyl-Thiophene

As shown above in Figure 5.2.1, prominent features in the experimental spectrum include the stretch of the bond between the pyridy and thiophene groups at 330 cm^{-1} and the concurrent ring-breathing mode of both pyridyl and thiophene at 703 cm^{-1}. Additional features of interest include the pyridyl ring breathing mode at 1000 cm^{-1} and the carbon-carbon double bond stretches of thiophene and pyridyl present at 1428 cm^{-1} and 1598 cm^{-1}, respectively. Shown below in Figure 5.2.2 is the optimized structure of the pyridyl-thiophene monomer.

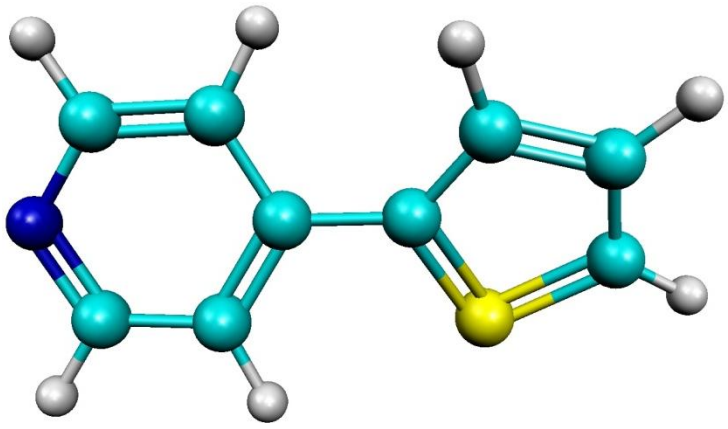

Figure 5.2.2: Optimized Structure of Pyridyl-Thiophene

The pyridyl-thiophene/C_6F_5I co-crystal Raman spectrum also included an emissive background that was removed for analysis of the vibrational features. For the co-crystal, an X-Ray crystal structure was also obtained. A portion of this crystal structure that clearly shows the halogen bonding is shown below in Figure 5.2.3.

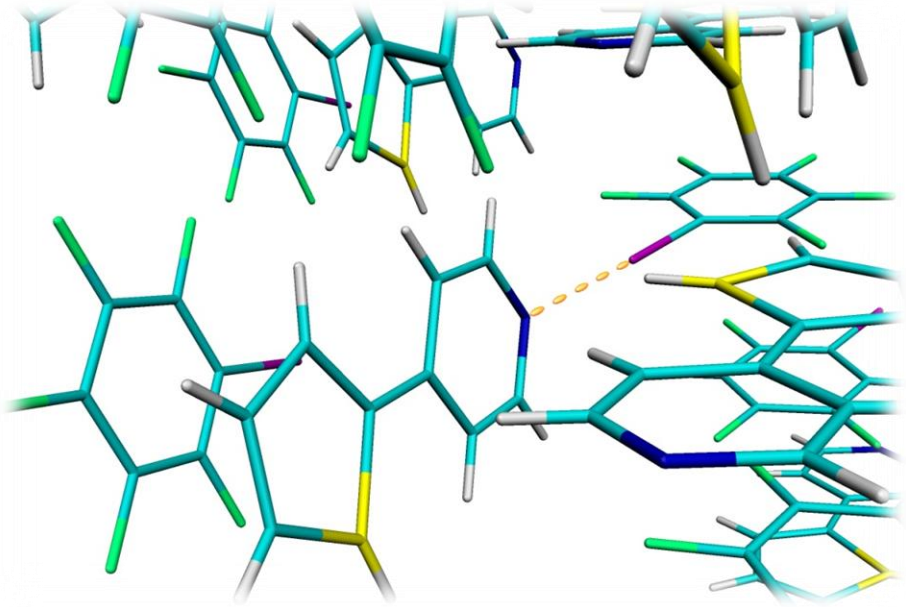

Figure 5.2.3: X-Ray Crystal structure of Pyridyl-Thiophene/C_6F_5I co-crystal

This crystal structure clearly shows that the pyridyl-thiophene monomer is completely planar, with iodine interacting with the nitrogen on the pyridyl group. This structure slightly differs from the optimized structure of pyridyl-thiophene that was obtained using Gaussian calculations. The optimized structure of the co-crystal using the M0-62X method and the def2-TZVPD basis set is shown below in Figure 5.2.4.

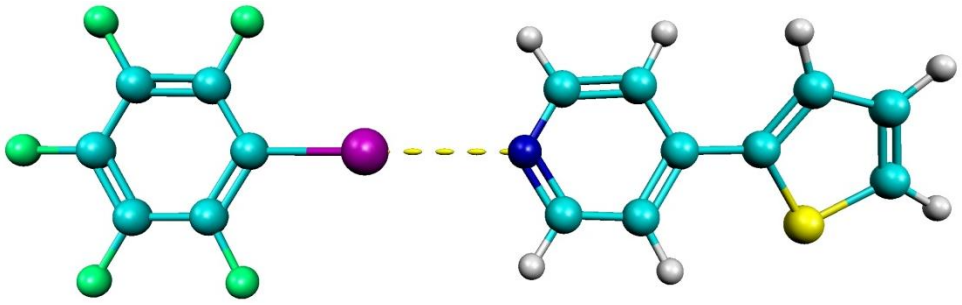

Figure 5.2.4: Optimized Structure of Co-Crystal

The optimized structure of the co-crystal using the M0-62X method and the def2-TZVPD basis set exhibit a near-planar structure with a slight rotation of the thiophene unit. This gas phase theoretical structure differs from the planar structure found using X-Ray crystallography. This is likely due to due intermolecular interactions present in the crystal structures, which are not accounted for in the optimization. The comparison of experiment to theory is shown below in Figure 5.2.5.

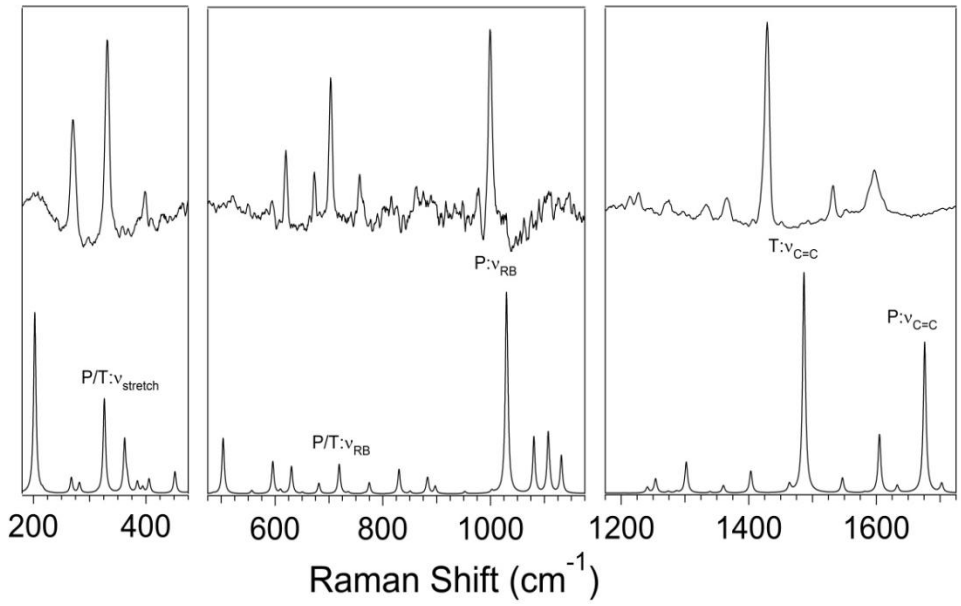

Figure 5.2.5: Comparison of Experiment to Theory of Co-Crystal

Despite the previously mentioned difference between the X-Ray crystal structure and the optimized theoretical structure, many experimental characteristics are recovered by theory. Agreement between experiment and theory was poorest at low energies and likely is due to additional intermolecular interactions in the crystal not taken into account by theory. The binding energy of the theoretical complex was also calculated and determined to be -6.79 kilocalories per mole. This high binding energy, similar to the binding energy observed in hydrogen bonded complexes, indicates that a strong non-covalent interaction is occurring in the system.

Comparison of pyridyl-thiophene and the co-crystal was carried out next. Comparison of the experimental pyridyl-thiophene Raman spectra and the Raman spectra of the co-crystal are shown below in Figure 5.2.6.

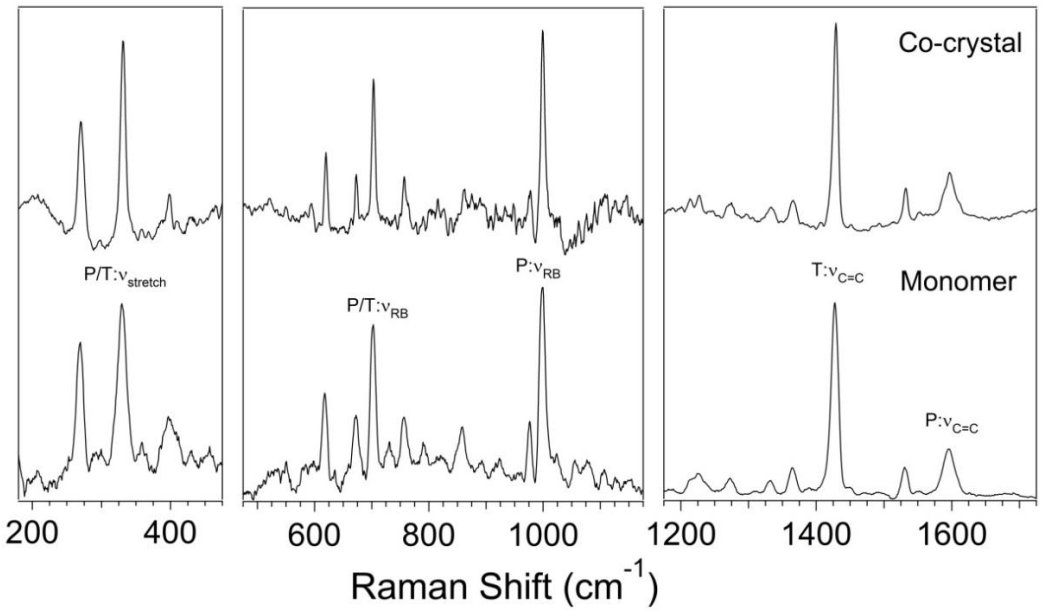

Figure 5.2.6: Comparison of Experimental Data of Pyridyl-Thiophene and Co-crystal

As can be seen by simply observing the spectra, it is difficult to see if there are any shifts occurring in the modes of pyridyl-thiophene. A closer analysis of the position of the peaks must be done in order to see if any shifts occurred. Experimental shift values for modes of pyridyl thiophene were determined, as well as theoretical shift values of these same modes. These experimental and theoretical shifts if vibrational modes of pyridyl-thiophene are shown below in Table 5.2.1.

Table 5.2.1: Experimental Shifts of Modes of Pyridyl-Thiophene in Co-Crystal (cm^{-1})

Pyridyl-Thiophene Peak Location	Co-crystal Peak Location	Experimental Shift	Theoretical Shift[6]
270	270	0	+4
330	331	+1	+7
397	398	+1	+3
618	620	+2	+4
671	673	+2	-2
703	703	0	+4
757	757	0	-1
999	1000	+1	+6
1332	1333	+1	1
1365	1366	+1	-4
1428	1429	+1	-1
1531	1532	+1	2
1596	1597	+1	1

Comparison of the experimental data showed small shifts in the modes of the pyridyl-thiophene monomer in the co-crystal. The blue shifts are small in magnitude, and it is difficult to attribute them directly to halogen bonding interactions. However, the X-Ray crystal structure did indicate that a halogen bonding interaction was occurring in the system. Additionally, theory did predict blue shifts in many of the same modes in which

[6] M062X/def2-TZVPD

they were observed experimentally, which shows that theory does agree with experiment in this case.

5.3 Conclusions

Characterization of pyridyl-thiophene and the pyridyl thiophene/ C_6F_5I co-crystal proved to be difficult due to the emissive background present in the experimental spectra. However, despite these difficulties, experimental Raman spectra were still able to be produced and graphed. Prominent peaks in both the monomer and co-crystal were able to be identified. Theoretical calculations produced an orientation of the pyridyl-thiophene unit different than what was determined using X-Ray crystallography. Despite this, agreement between experiment and theory was still good, with only a few slight differences. The binding energy of the co-crystal complex, -6.79 kilocalories per mole, indicates that a strong non-covalent interaction is occurring in the system. Comparison of experimental data of the pyridyl-thiophene monomer to experimental data of the co-crystal incorporating C_6F_5I showed small blue shifts which are difficult to directly contribute to a halogen bonding interaction; however evidence presented in the X-Ray crystal structure indicates that there is a halogen bond formed in the co-crystal.

List of References

1. Hobza, P. a. M.-D., Klaus, *Non-Covalent Interactions Theory and Experiment*. 2010.

2. Desiraju, R. G. What is a weak hydrogen bond? http://www.icmr.ucsb.edu/programs/archive/documents/Desiraju2.pdf (accessed 25 March 2015).

3. Clark, T.; Hennemann, M.; Murray, J. S.; Politzer, P., Halogen bonding: The σ-hole: Proceedings of "Modeling interactions in biomolecules II", Prague, September 5th-9th, 2005. *Journal of Molecular Modeling* **2007,** *13* (2), 291-296.DOI: 10.1007/s00894-006-0130-2

4. Carlsson, A.-C. C.; Gräfenstein, J.; Budnjo, A.; Laurila, J. L.; Bergquist, J.; Karim, A.; Kleinmaier, R.; Brath, U.; Erdélyi, M., Symmetric Halogen Bonding Is Preferred in Solution. *Journal of the American Chemical Society* **2012,** *134* (12), 5706-5715.DOI: 10.1021/ja301341h

5. Metrangolo, P.; Murray, J. S.; Pilati, T.; Politzer, P.; Resnati, G.; Terraneo, G., The fluorine atom as a halogen bond donor, viz. a positive site. *CrystEngComm* **2011,** *13* (22), 6593-6596.DOI: 10.1039/c1ce05554b

6. Weiss, R.; Schwab, O.; Hampel, F., Ion-Pair Strain as the Driving Force for Hypervalent Adduct Formation between Iodide Ions and Substituted Iodobenzenes: Structural Alternatives to Meisenheimer Complexes. *Chemistry – A European Journal* **1999,** *5* (3), 968-974.DOI: 10.1002/(sici)1521-3765(19990301)5:3<968::aid-chem968>3.0.co;2-l

7. Riley, K. E.; Murray, J. S.; Fanfrlík, J.; Řezáč, J.; Solá, R. J.; Concha, M. C.; Ramos, F. M.; Politzer, P., Halogen bond tunability I: The effects of aromatic fluorine substitution on the strengths of halogen-bonding interactions involving chlorine, bromine, and iodine. *Journal of Molecular Modeling* **2011,** *17* (12), 3309-3318.DOI: 10.1007/s00894-011-1015-6

8. Valerio, G.; Raos, G.; Meille, S. V.; Metrangolo, P.; Resnati, G., Halogen Bonding in Fluoroalkylhalides: A Quantum Chemical Study of Increasing Fluorine Substitution. *The Journal of Physical Chemistry A* **2000,** *104* (8), 1617-1620.DOI: 10.1021/jp993415j

9. Voth, A. R.; Hays, F. A.; Ho, P. S., Directing macromolecular conformation through halogen bonds. *Proceedings of the National Academy of Sciences* **2007,** *104* (15), 6188-6193.DOI: 10.1073/pnas.0610531104

10. Auffinger, P.; Hays, F. A.; Westhof, E.; Ho, P. S., Halogen bonds in biological molecules. *Proceedings of the National Academy of Sciences of the United States of America* **2004,** *101* (48), 16789-16794.DOI: 10.1073/pnas.0407607101

11. Metrangolo, P.; Neukirch, H.; Pilati, T.; Resnati, G., Halogen Bonding Based Recognition Processes: A World Parallel to Hydrogen Bonding†. *Accounts of Chemical Research* **2005,** *38* (5), 386-395.DOI: 10.1021/ar0400995

12. Hassel, O., Structural Aspects of Interatomic Charge-Transfer Bonding. *Science* **1970,** *170*, 497-502.DOI: 10.1126/science.170.3957.497

13. Metrangolo, P.; Resnati, G., Halogen Bonding: A Paradigm in Supramolecular Chemistry. *Chemistry – A European Journal* **2001,** *7* (12), 2511-2519.DOI: 10.1002/1521-3765(20010618)7:12<2511::aid-chem25110>3.0.co;2-t

14. Guthrie, F., XXVIII.?On the iodide of iodammonium. *Journal of the Chemical Society* **1863,** *16* (0), 239.DOI: 10.1039/js8631600239

15. Remsen, I. N., J. F., The Action of Halogens on the Methylamines. *American Chemical Journal* **1896,** *18*, 90-95.DOI:

16. Robinson, J. W., Skelly Frame, Eileen M., Frame II, George M. , *Undergraduate Instrumental Analysis*. CRC Press: Boca Raton, FL, 2014; Vol. 7.

17. McHale, J. L., *Molecular Spectroscopy*. 1999.

18. Engel, T., Reid, Phillip, *Physical Chemistry*. Pearson Education: 2013; Vol. 3.

19. Frisch, M. J.; Trucks, G. W.; Schlegel, H. B.; Scuseria, G. E.; Robb, M. A.; Cheeseman, J. R.; Scalmani, G.; Barone, V.; Mennucci, B.; Petersson, G. A.; Nakatsuji, H.; Caricato, M.; Li, X.; Hratchian, H. P.; Izmaylov, A. F.; Bloino, J.; Zheng, G.; Sonnenberg, J. L.; Hada, M.; Ehara, M.; Toyota, K.; Fukuda, R.; Hasegawa, J.; Ishida, M.; Nakajima, T.; Honda, Y.; Kitao, O.; Nakai, H.; Vreven, T.; Montgomery Jr., J. A.; Peralta, J. E.; Ogliaro, F.; Bearpark, M. J.; Heyd, J.; Brothers, E. N.; Kudin, K. N.; Staroverov, V. N.; Kobayashi, R.; Normand, J.; Raghavachari, K.; Rendell, A. P.; Burant, J. C.; Iyengar, S. S.; Tomasi, J.; Cossi, M.; Rega, N.; Millam, N. J.; Klene, M.; Knox, J. E.; Cross, J. B.; Bakken, V.; Adamo, C.; Jaramillo, J.; Gomperts, R.; Stratmann, R. E.; Yazyev, O.; Austin, A. J.; Cammi, R.; Pomelli, C.; Ochterski, J. W.; Martin, R. L.; Morokuma, K.; Zakrzewski, V. G.; Voth, G. A.; Salvador, P.; Dannenberg, J. J.; Dapprich, S.; Daniels, A. D.; Farkas, Ö.; Foresman, J. B.; Ortiz, J. V.; Cioslowski, J.; Fox, D. J. *Gaussian 09*, Gaussian, Inc.: Wallingford, CT, USA, 2009.

20. Jensen, J. H., *Molecular Modeling Basics*. CRC Press: 2010.

21. Becke, A. D., A new mixing of Hartree–Fock and local density-functional theories. *The Journal of Chemical Physics* **1993,** *98* (2), 1372-1377.DOI: doi:http://dx.doi.org/10.1063/1.464304

22. Becke, A. D., Density-functional thermochemistry. III. The role of exact exchange. *The Journal of Chemical Physics* **1993,** *98* (7), 5648-5652.DOI: doi:http://dx.doi.org/10.1063/1.464913

23. Gaussian 09 User's Reference: Freq Keyword. (accessed 19 April 2015).

24. Howard, A. A.; Tschumper, G. S.; Hammer, N. I., Effects of hydrogen bonding on vibrational normal modes of pyrimidine. *Journal of Physical Chemistry A* **2010,** *114* (25), 6803-6810.DOI: 10.1021/jp101267w

25. Sarau, G. B., Arne; Lewandowska, Renata; Christiansen, Silke. From Micro– to Macro–Raman Spectroscopy: Solar Silicon for a Case Study *Advanced Aspects of Spectroscopy* [Online], 2012.

26. Feller, D., The role of databases in support of computational chemistry calculations. *Journal of Computational Chemistry* **1996,** *17* (13), 1571-1586.DOI: 10.1002/(sici)1096-987x(199610)17:13<1571::aid-jcc9>3.0.co;2-p

27. Feller, D.; Schuchardt, K. L.; Didier, B. T.; Elsethagen, T.; Sun, L.; Gurumoorthi, V.; Chase, J.; Li, J., *BASIS Set Exchange (BSE): Chemistry Basis Sets from the William R. Wiley Environmental Molecular Sciences Laboratory (EMSL) Basis Set Library*. p Medium: ED.

28. Zhao, Y.; Truhlar, D., The M06 suite of density functionals for main group thermochemistry, thermochemical kinetics, noncovalent interactions, excited states, and transition elements: two new functionals and systematic testing of four M06-class functionals and 12 other functionals. *Theor Chem Account* **2008,** *120* (1-3), 215-241.DOI: 10.1007/s00214-007-0310-x